Solar Energy Materials & Solar Cells 230 (2021) 111234

Contents lists available at ScienceDirect

Solar Energy Materials and Solar Cells

journal homepage: www.elsevier.com/locate/solmat

Advances in upconversion enhanced solar cell performance

Amr Ghazy [a], Muhammad Safdar [a,b], Mika Lastusaari [c], Hele Savin [d], Maarit Karppinen [a,*]

[a] Department of Chemistry and Materials Science, Aalto University, FI-00076, Espoo, Finland
[b] Picosun Oy, Tietotie 3, FI-02150, Espoo, Finland
[c] Department of Chemistry, University of Turku, FI-20014, Turku, Finland
[d] Department of Electronics and Nanoengineering, Aalto University, FI-00076, Espoo, Finland

ARTICLE INFO

Keywords:
Solar cells
Upconversion
Luminescence
Lanthanides
Atomic layer deposition
Photonics

ABSTRACT

Photovoltaics (PV) is the leading renewable energy harvesting technology. Thus, there is a remarkable strive to enhance the light harvesting capability of the state-of-the-art solar cells. The major issue common to all solar cell types is that they utilize only a limited portion of the solar spectrum, mostly in the visible range, as the active semiconductor materials suffer from intrinsic light absorption thresholds. As a result, photons below and above these threshold values do not contribute to the electricity generation. A plausible solution to enhance the performance is to integrate the PV cell with an upconverting (UC) component capable of harvesting lower energy photons in the infrared (IR) range and emitting visible light. The concept was first introduced in 1990s, but major progress in the field has been made in particular in the recent few years. In this overview our intention is to provide the readers with a comprehensive account of the progress in the research on the UC-enhanced solar cells. Lanthanide ions embedded in different host lattices constitute the most important UC material family relevant to the PV technology; we first summarize the design principles and fabrication routes of these materials. Then discussed are the different approaches taken to integrate the UC layers in actual PV device configurations. Finally, we will highlight the most prominent results obtained, give some future perspectives and outline the remaining challenges in this scientifically intriguing and application-wise important field.

1. Introduction

The expected global transition to sustainable energy has massively increased the demand for renewable energy sources such as the solar energy. The production of solar cells for the photovoltaics (PV) industry has been growing constantly already for several decades, and the prospects promise continuous growth in future too [1]. The most common solar cells are based on semiconducting materials and in order to convert solar energy into electricity as efficiently as possible, it is important to choose a semiconductor material with an appropriate band gap that matches the solar spectrum. However, a single material can be optimal only for a specific wavelength range and consequently, the solar cell materials are often divided into different categories based on the corresponding material properties.

The dominant technology category today in the PV market is based on crystalline silicon (c-Si). This is due to the abundancy of the raw material as well as the highly developed mass-production infrastructure that have benefitted from the silicon microfabrication development. Silicon has also a rather ideal band gap (1.1 eV), which matches well with the maximum-intensity wavelength of the solar spectrum. Consequently, c-Si cells have a theoretical power conversion efficiency limit of ~30% [2]; the experimentally confirmed photoconversion efficiencies are already close to this limit, the current record being 26.7% [3]. In addition to c-Si, so-called thin-film solar cells have a long history. Among this category, amorphous silicon (a-Si) has been studied a lot since it was first reported by Carlson and Wronski in 1976 [4]. These a-Si cells have a wide band gap (~1.8 eV) making the technology ideal for specific applications including indoors use, although the total power conversion efficiency has remained at a modest level of ~12% [2].

More recently, new materials have emerged as potential alternatives to replace the silicon-based cells. First, dye sensitized solar cells (DSSC) were invented in 1991 by O'Regan and Grätzel aiming to provide much lower material costs combined with a cheap and simple manufacturing technology [5]. More recently, an organohalide perovskite sensitizer in a DSSC cell was reported in 2009 [6], and as a result so-called perovskite solar cells (PSC) emerged as a sub-branch of the DSSC technology. Initially the power conversion efficiency in these emerging technologies was rather low, around 3–4% [7], but the growth has been enormous in

* Corresponding author.
E-mail address: maarit.karppinen@aalto.fi (M. Karppinen).

https://doi.org/10.1016/j.solmat.2021.111234
Received 27 April 2021; Received in revised form 5 June 2021; Accepted 7 June 2021
Available online 20 June 2021

a relatively short time; the highest conversion efficiency of over 20% was reported already in 2015 [8]. While these results are highly promising, there are still issues related to upscaling the technology and the long-term stability as compared to the state-of-the-art silicon-based solar cells.

Despite the progress made in enhancing the performance of the different solar cell technologies, the fundamental issues related to the semiconductor materials themselves (in particular their band gaps) still restrict the conversion efficiency prospects of the PV technology. Firstly, the photons with a higher energy than the band gap, i.e. the solar radiation often in the ultraviolet (UV) range, result in so-called charge carrier thermalization, which causes major energy losses as heat [9]. Another major loss mechanism is the limited absorption of the state-of-the-art PV semiconductors in the photon wavelengths below the band gap, typically in infrared (IR) part of the solar spectrum [10]. The upper wavelength limit for the IR absorption varies with the solar cell type according to its semiconductor material (Fig. 1) [11,12]. The c-Si solar cells have the smallest band gap which allows them to absorb up to 1100 nm of the solar radiation, but even these cells incur more than 19% loss in efficiency due to this incapability to fully utilize the IR part of the solar spectrum. For other types of solar cells, these losses are even higher, amounting up to 50% [10].

Traditionally, the aforementioned losses (both above and sub-bandgap) have been addressed by stacking multiple materials on top of each other with varying band gaps. Such multi-junction cells, often based on III-V semiconductors, have reached higher power conversion efficiencies even above 47% [13]. However, this technology category suffers from high fabrication and material costs and typically highly concentrated sunlight is needed to reach such high efficiencies. Recently, pricewise a more competitive technology emerged that combines only two different materials, hence the name tandem cells. Currently the most promising option seems to be to combine c-Si and perovskite solar cells. Some commercial activities are already established around this approach [14].

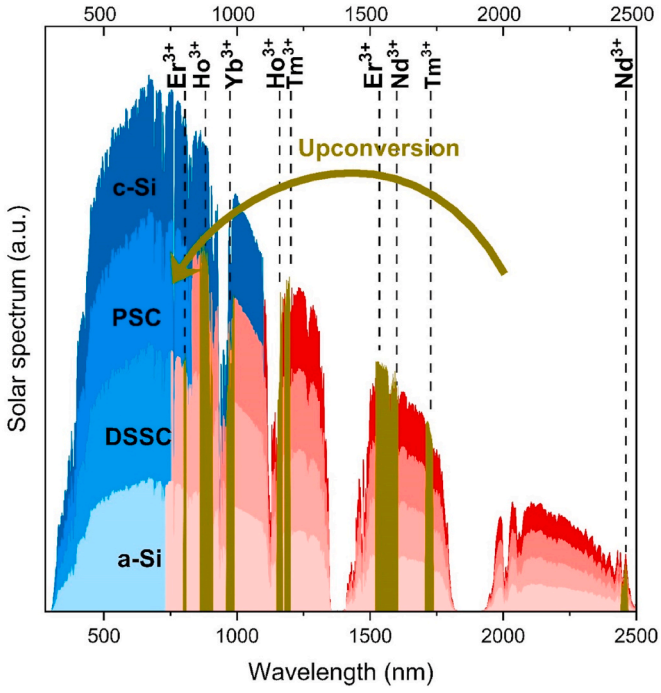

Fig. 1. Parts of the solar spectrum utilized (in blue) and lost (in red) of different solar cell types, and the absorption ranges (in green) of the upconverting Ln^{3+} ions, sketched according to Ref. [10]. (For interpretation of the references to colour in this figure legend, the reader is referred to the Web version of this article.)

An alternative means for the utilization of non-absorbed sub-band gap photons is to take advantage of so-called photon upconversion (UC) materials. Instead of having charge-collection junction made of a low band gap material, they are based on separate luminescent materials that are placed in the vicinity of the charge-collection structures. Upconversion is an anti-Stokes luminescence process exhibited by certain materials that are capable of absorbing low-energy photons typically in the near-infrared (NIR) range and then converting the energy into higher energy photons, typically in the visible (Vis) range. This phenomenon has shown immense potential towards several applications, including bioimaging, photodynamic therapy, sensors and display technology [15–18]. Regarding PV applications, the UC materials could considerably enhance the energy harvesting capability of the PV cells as they extend the useable solar spectrum range to the NIR photons in single junction solar cells (Fig. 1). A clear advantage of this approach is that no major adjustments or changes are needed for the current PV technologies to integrate them with the UC layers [19]. Indeed, upconversion in photovoltaics has already been demonstrated in several PV technologies, e.g. first in GaAs solar cells by Gibart et al. [20], later in c-Si cells by Trupke et al. [9], and most recently also in DSSCs by Shan and Demopoulos [21]. It is interesting to note that before the UC phenomenon itself was demonstrated experimentally, its use was suggested theoretically for the detection of infrared quanta in an IR quantum counter. That is essentially exactly what the PV-UC combination is set to do, to detect IR photons.

In recent years, several reviews have been published that discuss the chemistry and synthesis of UC materials [22], strategies used to tune the UC emission [23], and the progress in UC-enhanced DSSC and perovskite solar cells [24,25]. In this review, our intention is to provide a brief but comprehensive account of the state-of-the-art and the future prospects of the UC materials in photovoltaics. Majority of the studies on the UC materials in the context of the PV technologies have involved lanthanide-based UC materials [26,27]. Therefore, we start by discussing the UC properties of different lanthanide ions and the host materials used for them in Section 2. Then, before addressing the state-of-the-art of UC-integrated solar cells in Section 4, we devote Section 3 for different approaches taken to integrate the UC layers in PV devices and evaluating the performance enhancement in practice. Finally, Section 5 is a short summary of the current state and an outlook for the future perspectives and challenges in this scientifically exciting and industrially important field.

2. Lanthanide-based upconverting materials

2.1. Upconversion of lanthanides

Lanthanides (Ln) are the group of 14 elements in the Periodic Table after lanthanum, starting from cerium (Z = 58) up to lutetium (Z = 71) with the $6s^2 5d^1 4f^n$ electron configuration. For all these elements, the trivalent state is the most stable, where the 6s and 5d orbitals are empty and the 4f orbitals are partially filled. The 4f orbitals are strongly shielded from the coordination environment by the more spatially extended 5s and 5p orbitals. Because of the shielding, the Ln^{3+} ions exhibit characteristic narrow-band emission (Fig. 2). Moreover, since the f–f transitions are parity forbidden (no change in dipole moment), the excited states have long lifetimes [28]. This is an essential feature for enabling the stacking of photons required for upconversion.

There are several mechanisms for Ln^{3+} based upconversion (Fig. 3). In the excited state absorption (ESA) mechanism, one Ln^{3+} ion sequentially absorbs two photons so that the first excitation yields a metastable intermediate state which then absorbs a second photon to emit a single high energy photon [29]. The energy transfer upconversion (ETU) mechanism comprises two Ln^{3+} ions, one of them being a sensitizer and the other acting as an activator. The sensitizer ion absorbs a photon to reach an excited metastable state and thereafter transfers the energy non-radiatively to the activator. While the activator is still in the

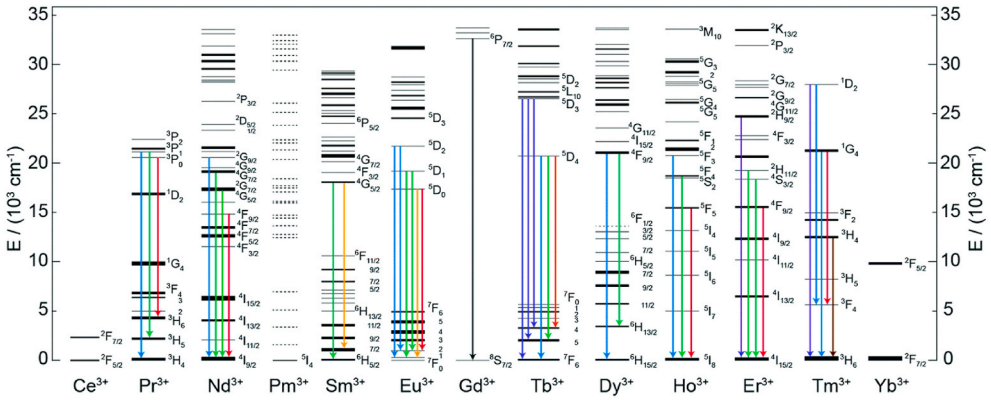

Fig. 2. Energy levels and emission lines seen for trivalent lanthanide ions [23].

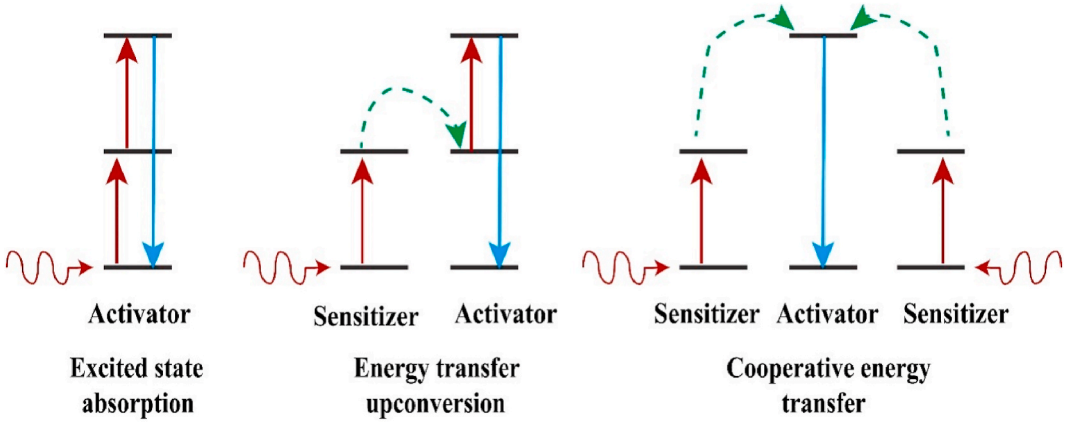

Fig. 3. Important UC mechanisms relevant for Ln^{3+} ions.

excited state, another photon absorbed by the sensitizer is transferred to the activator, which is then excited to a higher excited state [30]. A radiative relaxation of the activator results in the emission of an upconverted higher energy photon. Typically, Yb^{3+} is used as a sensitizer due to its high absorption cross-section, and the position of its f-f transition that lies around 980 nm, which facilitates energy transfer to the most common activator ions, e.g. Er^{3+}, Ho^{3+} and Tm^{3+} [31]. In the third UC mechanism, i.e. cooperative energy transfer (CET), two sensitizers individually absorb low energy photons and simultaneously transfer their energy to the activator to cooperatively excite it for a subsequent emission of the upconverted photon [32,33].

2.2. Host materials and synthesis strategies

The interest towards lanthanide luminescence started already in the 1880s [34], and during the 1940s, 1950s and 1960s the theoretical background was formulated. Since those times, numerous different compounds doped with lanthanides have been synthesized just for the sake of basic research. After the establishment of the UC phenomenon in the 1960s also upconversion has been reported in a wealth of different Ln-based materials [26]. In fact, the following efficient lanthanide luminescence hosts (where the Ln host is typically Y, La, Gd, or Yb) were characterized for (Yb^{3+},Er^{3+}) UC emission already by the early 1970s [35]: LnF_3, $LiLnF_4$, $NaLnF_4$, $BaLnF_4$, LnOX (X = F, Cl, Br), Ln_2O_3, $LnBO_3$, $YAlO_3$, $YGaO_3$, Ln_3BO_6, $Y_3Al_5O_{10}$, $Y_3Ga_5O_{10}$, Y_2GeO_5, Y_2GeO_7, $YTiO_5$, $Y_2Ti_2O_7$, YPO_4, $YAsO_4$, YVO_4, $YTaO_4$, $LnNbO_4$, Y_3TaO_7, Y_3NbO_7, YTa_3O_9, YNb_3O_9, Y_2TeO_6, Y_2WO_6, and $NaLn(WO_4)_2$. In practice, all materials that can be doped with lanthanides can also be doped with e.g. Yb^{3+}, Er^{3+}, Ho^{3+} and Tm^{3+} to obtain the UC emission with at least some intensity.

In a practical UC material, where the Ln^{3+} ions are embedded in a suitable host lattice, the crystal structure and composition of this host lattice lay the grounds for the UC efficiency by affecting the site symmetry of the lanthanides and offering suitable energy transfer routes as well as inhibiting the radiation-less de-excitation. Also, the absorption cross-sections, concentrations and homogeneity in distribution of the lanthanide dopants affect the UC properties of the material [12]. To allow easy doping of the Ln^{3+} ions, at least one of the cation species in the host lattice should be of similar size, and preferably also valence, to the Ln^{3+} dopants. An important requirement for the host lattice is that it provides an asymmetrical crystal field to allow the f-f transitions of the Ln^{3+} ions [36]. Also, an optimal host material should possess low phonon energies to minimize the non-radiative emissions [34], and be thermally and chemically stable, and transparent to the IR photons [35]. One possibility for such thermally and chemically stable host lattices are metal oxides, but the drawback is their high phonon energy. On the other hand, metal fluorides have been recognized as more efficient host material candidates owing to their lower phonon energy. In a very early review, the upconversion pioneer Auzel [35] demonstrated that the best fluorides may be even 100-fold more efficient in UC emission than the best oxides. Unfortunately, the fluorides are often hygroscopic, which may be a limitation [37]. For example, YF_3:Yb^{3+},Er^{3+} was initially proven to yield four times as high UC efficiency as $NaYF_4$:Yb^{3+},Er^{3+} [38], but the less hygroscopic tetrafluoride has established a position as the leading UC host. This flagship material was first highlighted in 1972 in two separate studies: by Menyuk et al. [39] for the cubic α-$NaYF_4$, and by Kano et al. [40] for the hexagonal β-$NaYF_4$. Due to its stronger UC emission, the hexagonal form is currently considered more promising [41], and thus it is being studied vigorously for many different fields of UC applications.

A common way to apply the Ln^{3+}-based UC materials is to synthesize them in nanoparticle form, motivated by the fact that in NPs the non-radiative losses are usually lower and the UC quantum yield higher [42]. However, the lattice strain, surface defects and solvent inclusion with high phonon energies may cause quenching of the UC luminescence [43]. To address these issues, specific core-shell NP structures have been developed [24]. In these CS-NPs, the UC core is isolated by an inert shell. The quality of the UC luminescence process may vary based on the shell characteristics, including the chosen material and the thickness [44]. In addition to different types of nanoparticles, UC materials are typically also produced e.g. as microcrystalline powder, thin films, glass and glass ceramics. In Table 1, we have collected some examples of recently investigated UC materials (matrix, dopants) and also their synthesis methods, and the form in which the material is applied. It is to be noted that in the time period 2017–2020, the number of scientific articles and proceedings papers dealing with UC has maintained a steady pace of ca. 2000 publications per year. Thus, the material list presented below is by no means exhaustive.

Recently, UC thin films have become more appealing and important due to their compatibility towards solid-state optical devices and applications. Thin films have been fabricated from UC NPs using solution-based methods such as spin-coating [45] and dip-coating [46], but the drawback is that the thus prepared films are prone to contain traces of solvent impurities. Alternately, gas-phase deposition techniques, such as metal-organic chemical vapor deposition (MO-CVD) and atomic layer deposition (ALD) [47], could provide an attractive way to produce precisely thickness-controlled UC thin films on a variety of substrates [48]. Such UC thin films can offer some unique features over the NPs, such as conformality and improved adhesion to the substrate in practical devices [49].

3. Integration of upconversion layers in solar cell devices

3.1. Integration strategies

Several ways of fabricating and incorporating the UC layer within the solar cell structure have been experimented. Typically, the UC material is produced in a powder or nanoparticle form (as summarized in Table 1), and then applied as a thin coating using e.g. spin-coating, dip-coating techniques, or deposited directly from gaseous precursors.

In Fig. 4, we show representative schemes for the placement of the UC layer within different PV cell types. For example, Markose et al. [52] used the coprecipitation method for synthesizing (Yb^{3+},Er^{3+})-doped Y_2O_3, YOF and YF_3 UC phosphors which were then integrated in a back reflector layer of thin-film a-Si solar cells fabricated through plasma-enhanced chemical vapor deposition (PECVD). In another investigation, (Yb^{3+},Ho^{3+})-doped Y_2O_3 UC layers were prepared solvothermally, and combined with N3 ($C_{26}H_{16}N_6O_8RuS_2$) dye-sensitized TiO_2-based DSSC cells fabricated by spin-coating; adding the UC layer was done by introducing the electrolyte solution by clamping both the FTO glass plates [87].

Li et al. [88] used pulsed laser deposition (PLD) technique to deposit $NaYF_4$:Yb^{3+},Er^{3+}/$NaYF_4$:Yb^{3+},Tm^{3+} (55-nm UC layer) on their PSC device. Most recently, we demonstrated the use of the ALD technique in depositing $(Er,Ho)_2O_3$ (45–60 nm UC layer) on a silicon substrate, which was mounted to the backside of a bifacial c-Si solar cell [49]. Using bifacial c-Si cells [89,90] in photon upconversion (as compared to fully metallized backside cells) [91,92] has the benefit that there is no need to adjust the commercial cell fabrication process at all but the upconversion layer can be just placed to the bottom of the finished cell. Additional back reflector can be used to guide the luminescent photons back to the cell.

It is important to note that a precise control over the film thickness of the UC layer is critical to achieve optimal UC emission [49,93,94]. Hence, the advanced gas-phase deposition techniques are clearly beneficial over the solution techniques as they allow for a nanoscale

Table 1
Examples of important host lattices for Ln-doped UC materials including the synthesis method and the form the material is applied: powder (P), nanoparticle (NP), core-shell nanoparticle (CS-NP), thin film (TF), glass/ceramics (G), or nanorod (NR).

Host material	Ln dopant	Form	Synthesis method	Ref.
Oxides				
Y_2O_3	Yb^{3+}, Er^{3+}, Eu^{3+}	P	Solvothermal	[50]
	Er^{3+}	P	Sol-gel	[51]
	Yb^{3+}, Er^{3+}	P	Co-precipitation	[52]
$(Yb,Er)_2O_3$	Yb^{3+}, Er^{3+}	TF	ALD	[48]
Er_2O_3	Ho^{3+}	TF	ALD	[49]
Lu_2O_3	Yb^{3+}, Er^{3+}	P, NP	Combustion	[53]
SiO_2	Yb^{3+}, Er^{3+}	TF	Dip-coating	[46]
SiO_2–TiO_2	Ho^{3+}	TF	Sol-gel & Spin-coating	[54]
	Yb^{3+}, Er^{3+}, Eu^{3+}	TF	Sol-gel	[55]
Au@TiO_2	Yb^{3+}, Er^{3+}	CS-NP	Hydrothermal	[56]
anatase-TiO_2	Yb^{3+}, Er^{3+}	TF	Sol-gel & Spin-coating	[45]
Mg_2SiO_4	Er^{3+}	TF	Co-precipitation	[57]
$Gd_{4.67}Si_3O_{13}$	Tm^{3+}	P	Solid state synthesis	[58]
$NaY_9(SiO_4)_6O_2$	Yb^{3+}, Tm^{3+}	P	Solid state synthesis	[59]
	Yb^{3+}, Ho^{3+}	P		
ZnO	Yb^{3+}, Er^{3+}	NP	Solution-combustion	[60]
$CaCe_2(MoO_4)_4$	Yb^{3+}, Er^{3+}	NP	Sol-gel	[61]
$Gd_{0.5}Na_{0.5}MoO_4$	Ho^{3+}, Yb^{3+}	NP	Co-precipitation	[62]
$SrAl_2O_4$	Eu^{3+}, Yb^{3+}	NR	Electrospinning	[63]
$Ba_{0.85}Ca_{0.15}Ti_{0.9}Zr_{0.1}O_3$	Er^{3+}	TF	Chemical solution deposition	[64]
TeO_2–GeO_2–Na_2O–Nb_2O_5–Er_2O_3	Er^{3+}	G	Melt-quenching	[65]
$NaBi(WO_4)_2$	Yb^{3+}, Er^{3+}	P	Solid state synthesis	[66]
$Na_8Al_6Si_6O_{24}(Cl,S)_2$	Yb^{3+}, Er^{3+}	P	Solid state synthesis	[67]
Oxyfluorides				
YOF	Yb^{3+}, Er^{3+}	P	Co-precipitation	[52]
$Y_2Te_6O_{15}$–BaF_2–YF_3	Yb^{3+}, Er^{3+}	G	Melt-quenching	[68]
Fluorides				
YF_3	Yb^{3+}, Er^{3+}	P	Co-precipitation	[52]
$NaYF_4$	Yb^{3+}, Er^{3+}	NP	Microemulsion	[69]
β-$NaYF_4$	Yb^{3+}, Tm^{3+}	TF	Sol-gel	[70]
$Cu_{1.8}S$@$NaYF_4$@$NaYF_4$	Yb^{3+}, Er^{3+}	CS-NP	Solvothermal	[71]
$NaYF_4$@$NaPO_3$–Na_2O–NaF	Yb^{3+}, Er^{3+}	NP in G	Melt-quenching	[72]
Li(Gd,Y)F_4	Yb^{3+}, Er^{3+}	NP	Thermal decomposition	[73]
$KLaF_4$	Yb^{3+}, Er^{3+}/ Tm^{3+}/ Ho^{3+}	NP	Solvothermal	[74]
$BaYF_5$		NP	Co-precipitation	[75]

(continued on next page)

Table 1 (*continued*)

Host material	Ln dopant	Form	Synthesis method	Ref.
	Yb^{3+}, Er^{3+}, Tm^{3+}			
Ba_2LaF_7	Nd^{3+}, Yb^{3+}	G	Melt-quenching	[76]
$NaGdF_4$@$NaGdF_4$@ZIF-8	Yb^{3+}, Er^{3+}	CS-NP/MOF	Solvothermal	[77]
PbF_2	Yb^{3+}, Er^{3+}, Ho^{3+}	P	Solid state synthesis	[78]
CaF_2	Yb^{3+}, Er^{3+}, Tm^{3+}	TF	MO-CVD	[79]
CaF_2	Yb^{3+}, Er^{3+}, Tm^{3+}	TF	MO-CVD Sol-gel	[80]
InF_3–ZnF_2–SrF_2–BaF_2	Er^{3+}	G	Melt-quenching	[81]
Others				
YPO LaPO$_4$ GdPO$_4$ LuPO$_4$	Yb^{3+}, Er^{3+}	NP		[82]
Al_2O_3–P_2O_5–SiO_2-Yb_2O_3	Yb^{3+}	G	Sol-gel	[83]
MoS_2	Yb^{3+}, Er^{3+}	P	Hydrothermal	[84]
Y-pyrazine	Yb^{3+}, Er^{3+}	TF	ALD/MLD	[85]
(Yb,Er)-IR-806	Yb^{3+}, Er^{3+}	TF	ALD/MLD	[86]

thickness control. The ALD technology in particular is highly promising owing to its unique characteristics, such as relatively mild deposition conditions and the large-area uniformity and conformality of the resultant thin films [47]. Moreover, ALD cycles for metal species can be combined with MLD (molecular layer deposition) cycles for organic molecules to grow amorphous or crystalline metal-organic materials [95,96], where the ultrathin organic layers could work e.g. for sensitization. The ALD and ALD/MLD techniques have already been used for the fabrication of various Ln-based thin films with interesting photoluminescence and upconversion properties [86,97–105] though mostly not yet integrated with actual solar cell structures.

3.2. Figures of merit

The evaluation of enhancement in solar cell performance due to upconversion can be reported with different indicators. From the final application point of view, the most informative parameter is naturally the power conversion efficiency (PCE), which describes the ratio between the energy produced by the solar cell and the input solar energy. Obviously, successful implementation of UC to the cells should be seen as higher PCE. However, PCE is affected by many different factors and it may hence be difficult to estimate the role of UC in the given cell architecture. Therefore, it is often more useful to focus on the cell parameters that measure directly the impact of the UC process as these describe better the potential of the given UC material.

One of such parameters is external quantum efficiency (EQE), which describes the ratio between the number of charge carriers (electrons) collected by a solar cell and the number of photons incident on the cell. EQE can be measured for each photon wavelength separately, which gives the advantage that one can focus on the EQE of the emitted photon wavelength originating from the luminescent material. For instance, in case of $NaYF_4$:Er^{3+}, the EQE is interesting only wavelength range of 1480–1560 nm [106–109]. If EQE is increased with the given wavelength, it means more charge carriers are generated and as a result the cell produces higher current. In fact, from the measured EQE one can calculate the short circuit current (I_{sc}) for the solar cell (or current density, J_{sc}, is often preferred as it is independent on the cell area). Alternatively, one can also directly measure J_{sc} by measuring the photocurrent of the cell under zero bias voltage. Since J_{sc} is the parameter that is affected directly by the incoming photons, it is the most widely used parameter to describe the effectiveness of the UC process on the cell efficiency.

The EQE (and J_{sc}) values are directly proportional to PCE, which means that only if all the other parameters remain unaffected, increase

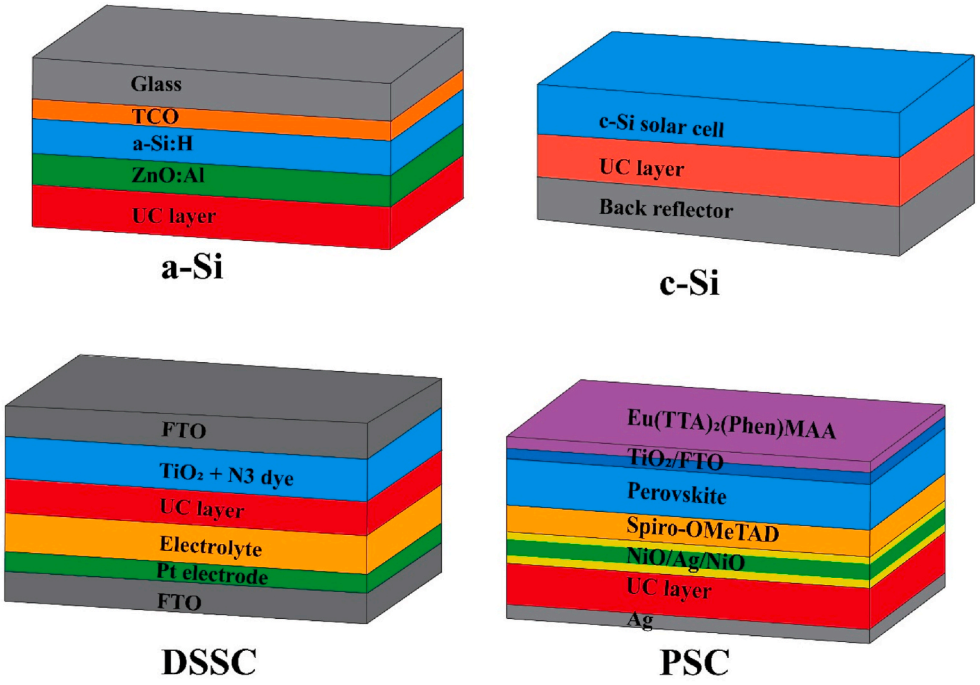

Fig. 4. Integration of UC layers in different solar cell types: a-Si (amorphous silicon), bifacial c-Si (crystalline silicon), DSSC (dye synthesized solar cell), and PSC (perovskite solar cell) [49,52,87,88]. (For interpretation of the references to colour in this figure legend, the reader is referred to the Web version of this article.)

in EQE or J_{sc} will be seen in PCE. Therefore, the EQE and J_{sc} values are much more informative parameters than PCE in convincing the community about the quality of the studied material in an UC process.

4. State-of-the-art of upconversion-integrated solar cells

The implementation of UC in solar cells is an area of increasing interest since last few decades. The first positive results were reported by Gibart et al., in 1996, when they combined (Yb^{3+},Er^{3+}) co-doped vitroceramic with an ultra-thin GaAs solar cell [20]. A sequential absorption and energy transfer of the IR photons from Yb^{3+} to Er^{3+} resulted in emission of a green photon that caused a photo-response in the 0.039 cm^2 substrate-free GaAs cell. With an input excitation of 1W at 1.39 eV by a Ti-sapphire IR laser, an EQE of 2.5% was measured. Later, integration of $NaYF_4$:Er^{3+} UC layers with bifacial c-Si solar cells was demonstrated [110]. The polycrystalline UC samples were mixed into an optically transparent acrylic adhesive with similar refractive index and coupled to the rear of a bifacial silicon solar cell. An EQE of about 2.5% was obtained under 5.1 mW excitation at 1523 nm. Trupke et al. [111] theoretically predicted up to ~40% conversion efficiency using non-concentrated sunlight (AM1.5) for a silicon solar cell combined with UC. However, a practical demonstration with $NaYF_4$:Er^{3+} UC phosphors gave an EQE close to 1% at 1550 nm, using a prototypical device setup. In recent years, the efforts in the field have rapidly grown to apply UC materials in different forms and combine UC with conventional as well as emerging solar cell technologies.

Amorphous silicon solar cells: As mentioned in the introduction, a-Si cells are relatively low-cost and easy to fabricate with an additional advantage of high chemical stability. The relatively wide band gap of a-Si (~1.8 eV) implies that these devices can absorb only up to 700 nm of solar light, hence they suffer from greater transmission losses compared to some other solar cell technologies, such as crystalline Si (c-Si). The research related to UC enhancement of a-Si cells can be traced back to 2010 [112–114], when de Wild et al. and Zhang et al. independently reported Er^{3+}-based $NaYF_4$ nanocrystals coupled to the backside of a-Si solar cells. De Wild et al. [112,113] used 200–300 μm thick layers of β-$NaYF_4$:Yb^{3+},Er^{3+} powder dispersed in polymethylmethacrylate (PMMA) and applied to the backside of a-Si cells using spin-coating; they recorded a 3x increase in the short-circuit current. On the other hand, Zhang et al. [114] implemented $NaYF_4$ nanocrystals with 18% Yb^{3+} and 2% Er^{3+} doping to achieve an increase of ~6% in short-circuit current density for their a-Si cells, as shown in Fig. 5. Later, Chen et al. [115] applied β-$NaYF_4$:Er^{3+} powder dispersed in cyclohexane to produce a 200 μm thick UC layer on a glass substrate, followed by physical placement of it below an a-Si cell. Under single-illumination with 60/80 mW/cm^2 980/1560 nm diode lasers, short-circuit currents of 0.3/0.01 μA were measured, respectively. Under co-excitation by 60 mW 980 nm and 100 mW 1560 nm lasers, a current improvement to 0.54 μA was obtained, owing to the UC-induced enhancement.

More recently, Markose et al. [52] investigated three different host lattices, Y_2O_3, YOF and YF_3, for (Yb^{3+},Er^{3+}) co-doping, and found YF_3 as the best matrix among the tested ones, for the performance enhancement of a-Si cells. An improvement of 7.5% in short-circuit current density was recorded for YF_3:Yb^{3+},Er^{3+} UC layers on AM1.5G along with a single wavelength diode laser source of 980 nm. Liu et al. [116] reported an enhancement of 25%, as shown in Fig. 5 in the short-circuit current for a thin film a-Si solar cell by applying (Yb^{3+},Er^{3+}) co-doped β-$NaYF_4$ dispersed in a PMMA layer.

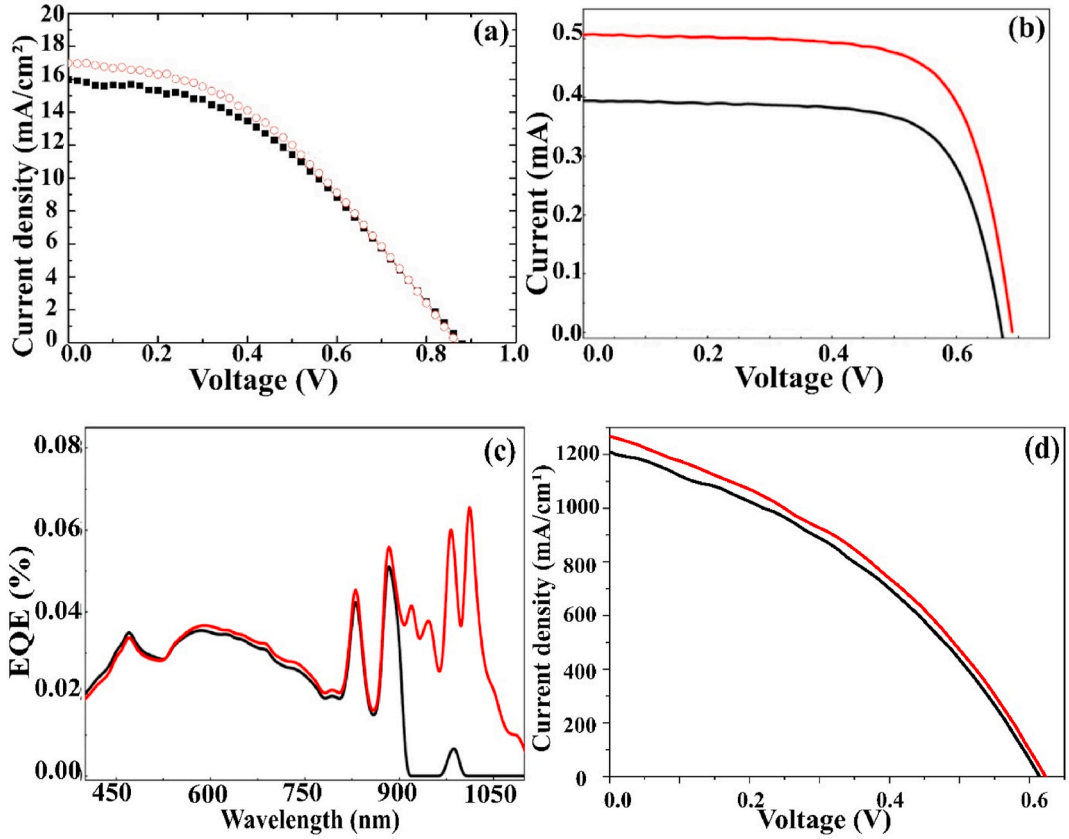

Fig. 5. (a) I–V curve of the pioneering work done in 2009 using Yb^{3+}, Er^{3+} co-doped β-$NaYF_4$ in enhancing the performance of a-Si solar cells under AM 1.5G irradiation [114]. (b) I–V curve showing a 25% relative enhancement in I_{sc} of a-Si solar cell by adding Yb^{3+}, Er^{3+} co-doped β-$NaYF_4$ UC layer [116]. (c) EQE curve of a-Si solar cell that shows a clear enhancement of the 900–1000 nm region absorption [116]. (d) Enhancement in the J_{sc} of a bifacial c-Si solar cell, achieved by introducing an ALD-grown UC $(Er_{0.95}Ho_{0.05})_2O_3$ thin-film layer [49]. Reference cells are in black and UC-assisted cells are in red. (For interpretation of the references to colour in this figure legend, the reader is referred to the Web version of this article.)

Crystalline silicon solar cells: The narrow band gap of c-Si (~1.1 eV) allows the c-Si cells to absorb photons up to 1100 nm. Hence, the employment of Yb^{3+}-based UC materials with the absorption maximum around 980 nm is not truly feasible; rather, other UC Ln ions should be challenged [117]. In this regard, Shalav et al. [86] in 2005 and Lahoz [94] in 2008 introduced Er^{3+}-doped $NaYF_4$ microcrystals and Ho^{3+}-doped oxyfluoride glass ceramics for expanding the absorption of c-Si solar cells into the sub-bandgap region. These ions absorb at 1150–1230 nm (Ho^{3+}) and 1450–1550 nm (Er^{3+}), and the emission of the UC photons takes place at <1000 nm. An attractive feature related to the use of Ho^{3+} (instead of e.g. Er^{3+}) is that the solar intensity at ~1180 nm is higher than at the longer wavelengths, indicating higher potential for the solar energy harvesting from this spectral range. An interesting idea is to use mixtures of two or more lanthanides in compatible concentrations to maximize the UC performance. For instance, (Ho^{3+},Yb^{3+}) co-doped UC materials can provide stronger NIR luminescence due to the inter-ion energy transfer and sensitization [118].

Fischer et al. [108] reported the use of Er^{3+}-doped BaY_2F_8 UC layers to reach 8% EQE under 1520 nm monochromatic excitation; the relative solar cell efficiency enhancement was 0.55 ± 0.14% at 94 ± 17 suns. Monocrystalline BaY_2F_8:Er^{3+} shows less scattering than the typically used microcrystalline powders such as β-$NaYF_4$:Er^{3+}. Incoming lower energy photons can enter deep into the monocrystalline material, resulting in higher extent of absorption from abroad spectral range. Considerably smaller enhancement in EQE, i.e. 0.4%, was achieved when Er^{3+} doped tellurite glass was combined with a c-Si cell under 1500 nm laser excitation [119]. More recently, we demonstrated a 3% improvement in short-circuit current density, as shown in Fig. 5, under a solar excitation equivalent to 16 suns, for a bifacial c-Si cell combined with ALD-grown $(Er_{0.95}Ho_{0.05})_2O_3$ thin film [49].

Dye sensitized solar cells: The power conversion efficiency of DSSCs depends on the band gap of the dye used; for the most commonly used ruthenium dye the band gap is ~1.8 eV, which averts the cells from absorbing light beyond ~800 nm. Thus, DSSCs inherently suffer from a low PCE [24], with the record in PCE being 14.7% from the year 2015 [120]. Hence, DSSCs are arguably the solar cell type that could benefit the most from the UC integration [10].

There are several approaches when incorporating the UC layers with DSSC, as seen in Fig. 6, one of them is adding the UC material to the TiO_2 layer. This approach was pioneered by Shan and Demopoulos in 2010 [21], who fabricated a DSSC cell by incorporating (Yb^{3+},Er^{3+}) co-doped LaF_3 with the TiO_2 layer of the cell. Recently, a similar approach was followed by Qin et al. [121] in their study where Ho^{3+}-doped $NaYbF_4$ was added to the TiO_2 layer, increasing the PCE of the cell from 5.84% to 7.52%, under one sun illumination.

Another route to integrate UC materials to DSSC devices is to add the UC component as a rear reflector functional layer, thus serving the two purposes of light harvesting and reflection simultaneously. In 2011, Liu et al. [124] added (Yb^{3+},Er^{3+}) co-doped $Y_3Al_5O_{12}$ layer as a back reflector, and demonstrated that 980 nm laser irradiation resulted in an enhanced J_{sc}. More recently, a remarkable 33.5% relative enhancement under one sun illumination was reported for a DSSC device in which the UC (Yb^{3+},Er^{3+}) co-doped CeO_2, used as a back reflector and scattering layer at the back of a DSSC, was additionally doped with Fe^{3+} [125].

An alternative approach is to employ the UC material as a counter electrode for the DSSC; this was reported by Li et al. [123] in 2014 who aimed to improve the performance of the cell using a lower cost counter electrode to replace Pt. Using (Yb^{3+},Er^{3+}) co-doped fluorine tin oxide (FTO) as a counter electrode they could achieve a relative enhancement of 24% in J_{sc} and increase the PCE from 6.7% to 7.30%, compared to a standard Pt electrode, under one sun illumination. More recently, a remarkable 68.5% relative enhancement compared to a standard UC-free Pt electrode was reported for a SnS-carbon counter electrode prepared using (Yb^{3+},Er^{3+}) co-doped CeO_2, raising the PCE of the DSSC from 5.65% to 9.52%, under one sun irradiation [126]. Interestingly, in the same study adding a similar UC layer to the Pt-electrode based DSSC raised the PCE of the cell to 8.32%, which translates to a 47.3% relative enhancement.

Perovskite solar cells: An attractive feature of PSCs is their large absorption coefficient [127]. However, the relatively wide band gap of ~1.55 eV of the most common material components in PSCs limits the absorption of such cells to ~780 nm. This, on the other hand, makes the PSCs an ideal target for the integration of UC materials to broaden the absorption range [128]. Upconversion-enhanced PSC was first reported by Chen et al. [129] in 2016, who added (Yb^{3+},Er^{3+}) co-doped $LiYF_4$ as an external light converting layer to the cell, to enhance the PCE by 7.9% under a 7–8 sun illumination, as shown in Fig. 7. The same technique was used more recently in a study where a plasmon-enhanced $NaYF_4$:Yb^{3+},Er^{3+}/$NaYF_4$:Yb^{3+},Tm^{3+}/Ag composite UC layer (Fig. 4) was found to enhance the PCE of the cell from 16.1% to 19.5% (21% increase), under one sun illumination [88]. Adding UC external layer to the rear side of the cell, showed better PCE enhancement than to the front side of

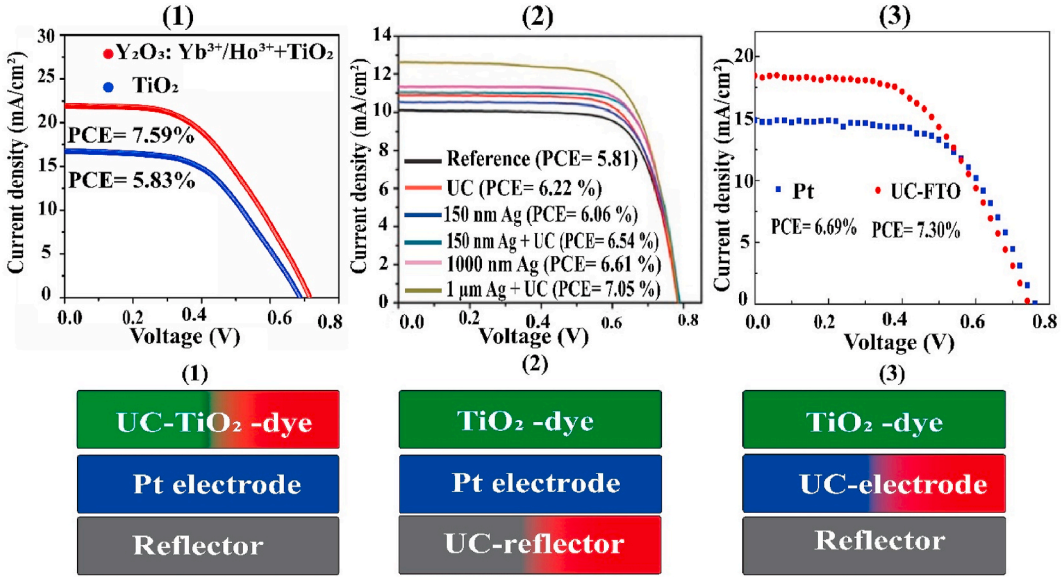

Fig. 6. I–V curves and schematic diagrams of UC assisted DSSC using different approaches; (1) incorporating the UC phosphor in the TiO_2 layer [87], (2) adding a UC rear reflector layer [122] and (3) replacing Pt counter electrode with a UC electrode [123].

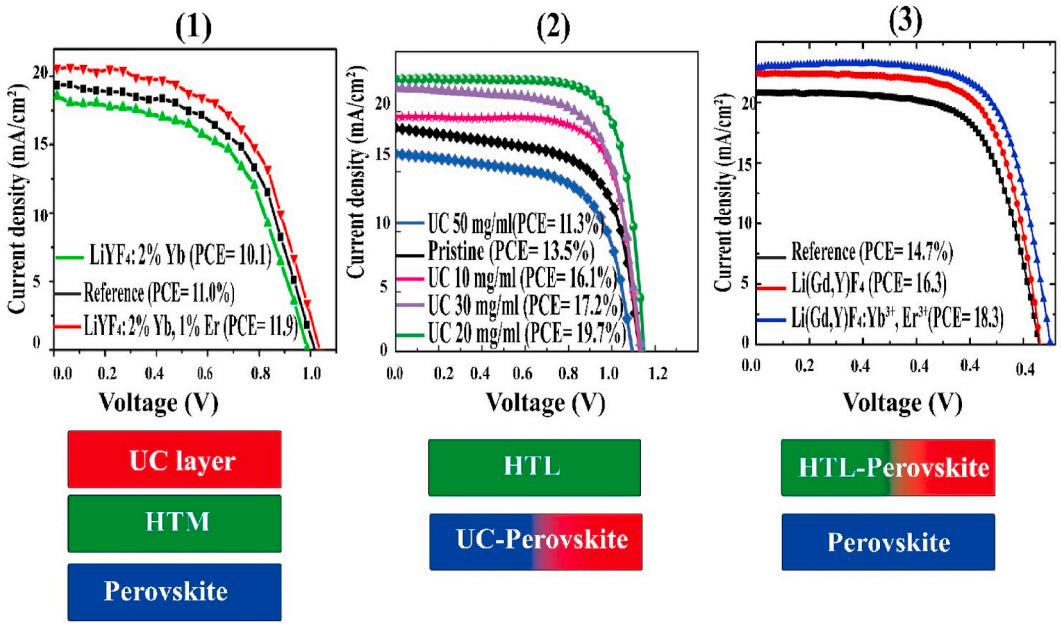

Fig. 7. I–V curves and schematic diagrams of UC assisted PSC using different approaches; (1) adding the UC as an additional active layer [129], (2) incorporating UC materials in the active perovskite layer [131], and (3) incorporating the UC material in the hole transport layer (HTL) of the cell [73].

the PSC [130].

Another approach is to incorporate the UC material in the perovskite active layer. This was demonstrated in 2017 by Meng et al. [131] using β-$NaYF_4$:Yb^{3+},Er^{3+} nanocrystals embedded within the perovskite layer in different amounts, raising the PCE of the cell from 12.1% to 18.60% as shown in Fig. 7 on average, to achieve a remarkable relative enhancement of 54.4% compared to the control device, under one sunlight illumination.

A third approach is to add the UC component to the hole transport layer of the PSC. This was explored by He et al. [132] who added β-$NaYF_4$:Yb^{3+},Er^{3+} to replace the mesoporous TiO_2 layer of the cell, thus raising the PCE of the cell from 12.88% to 17.78%, under one sun illumination; an additional 0.35% increase in PCE was obtained by 980 nm laser irradiation. Later, Deng et al. [73] used the same technique adding UC Li(Gd,YF_4:Yb^{3+},Er^{3+} nano crystals with different concentrations, to a PSC, increasing the PCE of the cell from 14.7% to 18.3% (Fig. 7) and achieving almost 25% relative enhancement compared to the undoped cell under simulated one sun illumination.

In Table 2, we have collected recent highlights of the solar cell performance enhancements achieved with the UC integration. As a general comment, it should be noted that the Ln^{3+} and transition metal (e.g. Fe^{3+}) dopants may, to certain extent, contribute to the observed enhancement due to their own photoluminescence effect.

5. Conclusions and outlook

In this brief overview, we have outlined the basic phenomena, material design issues and integration strategies related to the utilization of upconversion materials for enhancing the performance of various types of solar cells through spectral manipulation. This research field has been strongly emerging in recent years, and for all the major types of solar cells promising results have already been reported. For example, a J_{sc} of 20.5 mA/cm^2 and 21.9 which reflects a ~79% and ~63% relative enhancement to respective control devices have been reported for DSSC [126,142], while for the PSC, J_{sc} has reached of 22.7 mA/cm^2, reflecting a ~40% relative enhancement than the control device [131]. Here the direct comparison of the given numbers may not be fully fair though, as there are various ways to measure and express the magnitudes of performance enhancements; indeed, establishment of a more standard way of discussing the UC-driven enhancements could be one of the development targets in future.

The progress in the field is impressive considering that originally the UC phenomenon was realized only with lasers yielding very high excitation photon densities, while the recent highlights for UC-enhanced solar cells have been demonstrated with actual sun light excitation. There is definitely still lot of space for improving the efficiency of the applied UC layers themselves. This research line should include not only the fine-tuning of the currently known UC materials but also innovative search for new UC host matrices.

Lanthanide ions embedded in different host lattices constitute the most important UC material family relevant to the PV technology. For the required capability of harvesting lower energy photons in the NIR range and emitting visible light, the most advantageous lanthanide ions are the heaviest ones: Yb^{3+}, Tm^{3+}, Er^{3+}, Ho^{3+}, and Nd^{3+}. In practice, most of the studies have involved the combination of Yb^{3+} and Er^{3+} with the main absorption in the range 800–1000 nm; this NIR harvesting range fits quite well with the intrinsic absorption capability of the PV cells based on the wide-bandgap semiconductors (perovskite, dye-sensitized and organic solar cells). On the other hand, in the case of Si-based cells this wavelength range is already well absorbed by the narrow-bandgap Si itself (absorbs well up to 1100 nm). For c-Si, instead of Yb^{3+}, e.g. Ho^{3+} together with Er^{3+} could be more appropriate for efficient UC enhancement. Indeed, the major NIR absorption bands for Ho^{3+} and Er^{3+} are in the 1150–1230 and 1450–1580 nm ranges. In future works, more precise tuning of the UC Ln^{3+} ion composition/concentration should be targeted for each solar cell type separately. Another future challenge could be to more precisely investigate and discuss the true causes of enhancements observed with the UC materials. In reality, only a fraction of the absorbed photons is converted to the UC luminescence, and besides the UC emission there is always also regular photoluminescence present. Within the solar spectrum, many of the energy states of lanthanides can be excited which may result in regular photoluminescence in the visible wavelengths. This is a challenge regarding the deeper understanding and interpretation of the experimental observations, but at the same time we should learn to take a full benefit of all the upconversion, downconversion and photoluminescence processes enabled by the different lanthanides (and even some d-block transition metals) to be able to harness all the possibilities for the best

Table 2
Recent highlights of UC-enhanced solar cells. (NG: Not given)

Host material	Ln dopant	Indicator	Irradiation	Ref. without UC	Relative enhancem.	Year/Ref
a-Si						
Y_2O_3 YOF YF_3	Yb^{3+},Er^{3+}	J_{SC}	98 suns	13.1	3.4% 4.8% 7.5%	2018 [52]
β-$NaYF_4$	Yb^{3+},Er^{3+}	I_{SC}-EQE (980 nm)	AM1.5G	0.4–0	25% -+0.05%	2018 [116]
TeO_2–PbF_2	Yb^{3+},Er^{3+}	EQE (980 nm)	NG	4.25	+10.6%	2014 [133]
β-$NaYF_4$	Yb^{3+},Er^{3+},Gd^{3+}	EQE (980 nm)	NG	0.02	+0.12%	2012 [134]
β-$NaYF_4$	Er^{3+}	J_{SC}	laser (980, 1560 nm)	NG	+0.3 μA, +0.1 μA,	2012 [115]
β-$NaYF_4$	Yb^{3+},Er^{3+}	I_{SC}	AM1.5G	0.4	25%	2010 [114]
β-$NaYF_4$	Yb^{3+},Er^{3+}	EQE (980 nm)	laser 980 nm	0.01	+0.02%	2010 [113]
β-$NaYF_4$	Yb^{3+},Er^{3+}	J_{sc}	laser 980 nm	0.005	+0.005	2010 [112]
c-Si						
$(Er,Ho)_2O_3$	Er^{3+},Ho^{3+}	I_{SC}	16 suns	1021	3%	2021 [49]
TeO_2–WO_3–ZrO_2–Er_2O_3	Er^{3+}	EQE (1500 nm)	laser 1500 nm	0.1	+0.3%	2017 [119]
BaY_2F_8	Er^{3+}	EQE (1520 nm)	94 suns	~0	+7.4%	2015 [108]
PbF_2	Er^{3+}	EQE (1560 nm)	NG	0	+0.38%	2014 [135]
β-$NaYF_4$	Yb^{3+},Er^{3+}	EQE (1523 nm)	77 suns	0	+3.4%	2014 [136]
β-$NaYF_4$	Er^{3+}	EQE (1500 nm)	~1 sun	0	+1.69%	2014 [107]
InF_3–$20ZnF_2$–$20SrF_2$–$20BaF_2$	Yb^{3+},Er^{3+}	EQE (1480 nm)	864 suns	0.4	+0.1%	2013 [106]
BaY_2F_8	Er^{3+}	EQE (1557 nm)	~62 suns	0	+6.5%	2013 [109]
β-$NaYF_4$	Er^{3+}	PCE	~1 sun	7.68	8.6%	2012 [137]
ZrF_4–BaF_2–LaF_3–AlF_3–NaF–InF_3	Er^{3+}	EQE (1540 nm)	NG	NG	+2.4%	2011 [138]
β-$NaYF_4$	Er^{3+}	EQE (1523 nm)	NG	0	+5.1%	2010 [139]
β-$NaYF_4$	Er^{3+}	EQE (1523 nm)	NG	0	+3.4%	2007 [140]
β-$NaYF_4$	Er^{3+}	EQE (1523 nm)	NG	0	+2.5%	2005 [110]
DSSC						
β-$NaYF_4$	Ho^{3+}	PCE	AM 1.5G	5.8	28.8%	2021 [121]
$BiYO_3$	Yb^{3+},Er^{3+}	PCE	1 Sun	5.7	8.2%	2021 [141]
$NaYbF_4$	Ho^{3+}	PCE	1 Sun	6.4	46.1%	2021 [142]
$CaWO_4$@TiO_2	Yb^{3+},Er^{3+}	PCE	1 Sun	6.9	21%	2020 [143]
$LiYF_4$	Yb^{3+},Er^{3+}	PCE	AM 1.5G	5.0	51.1%	2020 [144]
Y_2O_3	Ho^{3+},Yb^{3+}	PCE	AM 1.5G	8.9%	10.3%	2020 [145]
CeO_2: Fe@TiO_2	Yb^{3+},Er^{3+}	PCE	AM 1.5G	5.5	33.5%	2020 [125]
YbF_3@TiO_2	Ho^{3+}	PCE	AM 1.5G	6.4	21%	2020 [146]
CeO_2	Yb^{3+},Er^{3+}	PCE	AM 1.5G	5.7	68.5%	2020 [126]
$La(OH)_3$ @TiO_2	Yb^{3+},Er^{3+}	PCE	AM 1.5G	6.4	38.0%	2019 [147]
$NaYF_4$ @TiO_2	Yb^{3+},Tm^{3+}	PCE	AM 1.5G	6.13	14.7	2019 [148]
Y_2O_3	Ho^{3+},Yb^{3+}	PCE	1 Sun	16.8–5.8	30.0%	2019 [87]
$NaYF_4$ @TiO_2	Yb^{3+},Er^{3+}	PCE	AM 1.5	5.5	31.6%	2019 [149]
$CaCe_2(MoO_4)_4$	Yb^{3+},Er^{3+}	PCE	AM 1.5	6.5	19.9%	2018 [61]
ZnO	Yb^{3+},Er^{3+}	PCE	AM 1.5G	8.3	8.3%	2018 [60]
β-$NaYF_4$	Yb^{3+},Er^{3+}	PCE	AM 1.5G	5.6	29.8%	2018 [150]
β-$NaYF_4$	Yb^{3+},Er^{3+}/Eu^{3+}	PCE	AM 1.5G	6.7	14.0%	2018 [151]
β-$NaYF_4$@YOF	Yb^{3+},Er^{3+}	PCE	AM 1.5G	7.0	17.1	2018 [152]
Y_2O_3@TiO_2	Er^{3+}	PCE	1 Sun	5.4	43.6%	2018 [153]
CeO_2	Yb^{3+},Er^{3+}	PCE	AM 1.5G	5.5	27.0%	2017 [154]
β-$NaYF_4$@SiO_2@TiO_2	Yb^{3+},Er^{3+}	PCE	AM 1.5G	5.6	16.6%	2017 [94]
Y_2O_3/Au@TiO_2	Er^{3+}	PCE	AM 1.5G	6.8	27.6%	2016 [155]
β-$NaYF_4$@β-$NaYF_4$	Yb^{3+},Er^{3+}	PCE	AM 1.5G	7.1	28.2%	2016 [156]
$NaYF_4$@SiO_2@Au@TiO_2	Yb^{3+},Er^{3+}	PCE	AM 1.5G	6.1	28.1%	2016 [157]
YbF_3/TiO_2	Ho^{3+}	PCE	AM 1.5G	6.5	24.6%	2016 [158]
Gd_2O_3	Yb^{3+},Ho^{3+}	PCE	1 sun	6.7	10.4%	2016 [159]
β-$NaGdF_4$	Yb^{3+},Er^{3+}	PCE	AM 1.5G	3.6	19.44%	2016 [160]
$Gd_2(MoO_4)O_3$	Yb^{3+},Er^{3+}	PCE	AM 1.5G	2.9	24.8%	2016 [161]
β-$NaYF_4$@SiO_2@TiO_2	Yb^{3+},Er^{3+}	PCE	AM 1.5G	8.67	5.0%	2016 [162]
β-$NaYF_4$	Yb^{3+},Er^{3+}	PCE	AM 1.5G	5.7	25.6%	2015 [163]
Y_2O_3, $Y_3Al_5O_{12}$	Er^{3+}, Ce^{3+}	PCE	AM 1.5G	5.2	35.4%	2015 [164]
β-$NaYF_4$@SiO_2	Yb^{3+},Er^{3+}	PCE	AM 1.5G	3.7	6.8%	2015 [165]
CeO_2	Yb^{3+},Er^{3+}	PCE	1 sun	5.8	15%	2015 [166]
β-$NaGdF_4$	Yb^{3+},Er^{3+}	PCE	AM 1.5G	6.8	11.3%	2015 [167]
β-$NaYF_4$	Yb^{3+},Er^{3+},Tm^{3+}	PCE	AM 1.5G	3.4	27.4%	2015 [168]
Y_2O_3	Yb^{3+},Er^{3+}	PCE	1 sun	5.9	12.5%	2015 [169]
ZnO/TiO_2	Yb^{3+},Er^{3+}	PCE	NG	3.0	35.8%	2015 [170]
β-$NaYF_4$@TiO_2	Yb^{3+},Er^{3+}	PCE	1 Sun	6.2	24.5%	2014 [171]
β-$NaYF_4$@ β-$NaYF_4$	Yb^{3+},Er^{3+}	PCE	AM 1.5G	5.0	5.9%	2014 [172]
β-$NaYF_4$@SiO_2	Yb^{3+},Er^{3+}	PCE	AM 1.5G	6.0	6.7%	2014 [173]
FTO	Yb^{3+},Er^{3+}	PCE	AM 1.5G	6.7	9.0%	2014 [123]
F-doped TiO_2	Yb^{3+},Er^{3+}	PCE	AM 1.5G	6.3	40.1%	2014 [174]
YF_3	Yb^{3+},Er^{3+}	PCE	AM 1.5G	5.3	26.6%	2014 [175]
β-$NaYF_4$@SiO_2@Au	Yb^{3+},Er^{3+}	PCE	AM 1.5G	7.2	14.8%	2014 [176]
β-$NaGdF_4$	Yb^{3+},Er^{3+}	PCE	AM 1.5G	5.8	21.4%	2014 [122]
β-$NaYF_4$@SiO_2@TiO_2	Yb^{3+},Er^{3+}	PCE	1 Sun	7.8	18.1	2013 [177]
TiO_2	Er^{3+}	PCE	AM 1.5G	4.1	62.9%	2013 [178]
$TiO_{2-x}F_x$	Yb^{3+},Er^{3+}	PCE	AM 1.5G	5.4	31.1%	2013 [179]

(*continued on next page*)

Table 2 (*continued*)

Host material	Ln dopant	Indicator	Irradiation	Ref. without UC	Relative enhancem.	Year/Ref
β-$NaYF_4$@TiO_2	Yb^{3+},Er^{3+}	PCE	AM 1.5G	3.5	23.1%	2013 [180]
β-$NaYF_4$	Yb^{3+},Er^{3+}	PCE	AM 1.5G	2.7	4.4%	2012 [181]
Y_2O_3	Yb^{3+},Er^{3+}	PCE	1 sun	5.8	19.9%	2012 [182]
$NaYF_4$	Yb^{3+},Er^{3+}	PCE	AM 1.5G	1.6	11.9%	2011 [183]
TiO_2	Yb^{3+},Er^{3+}	PCE	AM 1.5G	6.4	13.6%	2011 [184]
Lu_2O_3	Yb^{3+},Tm^{3+}	PCE	1 sun	6.0	11.1%	2011 [185]
β-$NaYF_4$	Yb^{3+},Er^{3+}	PCE	AM 1.5G	5.5	26.6%	2011 [186]
YF_3	Yb^{3+},Er^{3+}	PCE	1 sun	5.8	35.5%	2011 [187]
$Y_3Al_5O_{12}$	Yb^{3+},Er^{3+}	J_{sc}	laser 980 nm	~0	0.2%	2011 [124]
LaF_3–TiO_2	Yb^{3+},Er^{3+}	I_{sc}	AM 1.5G	6.2	2.4%	2010 [21]
PSC						
$NaCsWO_3$@ β-$NaYF_4$@β-$NaYF_4$	Yb^{3+},Er^{3+}	PCE	AM 1.5G	16.1	18.0%	2021 [188]
IR783: $NaYF_4$@$NaYF_4$	Yb^{3+},Er^{3+},Nd^{3+}	PCE	AM 1.5G	19.4	5.6%	2020 [189]
TiO_2	Yb^{3+},Er^{3+}	PCE	AM 1.5G	8.3	16.5%	2020 [190]
β-$NaYF_4$@$NaYF_4$	Yb^{3+},Er^{3+},Sc^{3+}	PCE	AM 1.5G	17.4	15.8%	2019 [191]
β-$NaYF_4$@SiO_2	Yb^{3+},Tm^{3+}	PCE	AM 1.5G	12.3	14.81%	2019 [192]
Li(Gd,Y)F_4	Yb^{3+},Er^{3+}	PCE	AM 1.5G	14.7	24.9%	2019 [73]
β-$NaYF_4$	Yb^{3+}, Tm^{3+}	PCE	AM 1.5G	15.8	15.2%	2019 [193]
TiO_2	Er^{3+}	PCE	AM 1.5G	9.1	16.5%	2018 [194]
β-$NaYF_4$	Ho^{3+}	PCE	AM 1.5G	11.1	29.0%	2018 [195]
KY_7F_{22}	Yb^{3+},Er^{3+}	PCE	AM 1.5G	13.2	6.1%	2018 [130]
TiO_2	Yb^{3+},Er^{3+}	PCE	AM 1.5G	14.0	17.9%	2018 [196]
β-$NaYF_4$@β-$NaYF_4$	Yb^{3+},Er^{3+},Tm^{3+}	PCE	AM 1.5G	16.1	19.3%	2018 [88]
β-$NaYF_4$@ SiO_2	Yb^{3+},Er^{3+}	PCE	AM 1.5G	8.2	21.1	2018 [197]
β-$NaYF_4$	Yb^{3+},Er^{3+}	PCE	AM 1.5G	13.5	46.4%	2017 [131]
TiO_2	Yb^{3+},Er^{3+}	PCE	AM 1.5G	10.3	20.8%	2017 [198]
β-$NaYF_4$/Li–Ag@SiO_2	Yb^{3+},Er^{3+}	PCE	AM 1.5G	7.8	33.4%	2017 [199]
β-$NaYF_4$-IRM06	Yb^{3+},Er^{3+}	PCE	AM 1.5G	13.5	29.4%	2017 [200]
m$Cu_{2-x}S_x$@SiO_2@Er_2O_3	Er^{3+}	PCE	AM 1.5G	16.2	9.9%	2017 [201]
$LiYF_4$	Yb^{3+},Er^{3+}	PCE	7-8 Suns	11	7.9%	2016 [129]
β-$NaYF_4$	Yb^{3+},Er^{3+}	PCE	AM 1.5G	12.9	9.8%	2016 [132]
β-$NaYF_4$	Yb^{3+},Er^{3+}	PCE	AM 1.5G	14.1	13.7%	2016 [202]
β-$NaYF_4$@β-$NaYF_4$	Yb^{3+}, Tm^{3+}	PCE	AM 1.5G	14.7	8.8%	2016 [203]
Others						
(QDSSC)TiO_2/CdS/β-$NaYF_4$	Yb^{3+},Er^{3+}	PCE	1 sun	2.14	106%	2020 [204]
(QDSSC)TiO_2	Yb^{3+},Er^{3+}	PCE	AM 1.5G	2.9	20%	2020 [205]
(GaAs) β-$NaYF_4$	Yb^{3+},Er^{3+}	PCE	AM 1.5G	7.9	68.4%	2018 [206]
(Polymer) β-$NaYF_4$	Yb^{3+},Er^{3+}	PCE	AM 1.5G	3.1	6.5%	2014 [207]
(Organic) β-$NaYF_4$	Yb^{3+},Er^{3+}	PCE	laser (980 nm)	0.0048	29.1%	2012 [208]
(Organic) Y_2BaZnO_5	Yb^{3+},Ho^{3+}	EQE (980 nm)	laser (980 nm) ~37 suns	0.2	+4.95%	2012 [209]
(GaAs) $Y_6W_2O_{15}$	Yb^{3+},Er^{3+}	I_{sc}	laser (973 nm)	0	+3.58 μA	2012 [210]
(GaAs) vitroceramic	Yb^{3+},Er^{3+}	PCE	NG	0	+2.5%	1996 [20]

possible utilization of these different energy conversion processes.

From the practical performance point of view, the era of UC-enhanced PV is yet in its infancy, considering how far we are from the possibly achievable maximum values. Among the different PV technologies, the market leading c-Si technology could turn out to be the most rewarding for the UC enhancement efforts in the sense that the performance of these cells is otherwise approaching a kind of saturation (current records around 27% versus the ~30% S-Q limit), meaning that the improvements expected through "standard" PV development efforts can be only fractional [211,212]. Optimistically, for the UC-enhanced c-Si PV technology the new target could be set much higher, even up to 40%, to truly shake the PV community.

From another perspective, it is difficult to see that the UC-enhanced solar cells could as such compete with the recent developments in the PV field, such as the tandem cells or new solar cell materials. Nevertheless, the UC components can be considered as a complementary technology which rather builds on top of the existing technologies providing extra boost to these technologies. A clear advantage is the relatively easy integration of the UC layers into the current PV cells, without drastically affecting the device configurations or process lines. Here the already existing strong c-Si PV infrastructure could be highly beneficial for the fast transition from the innovation to the commercial large-scale utilization.

Finally, we like to emphasize the importance of the fabrication technique of the UC layers/coatings. The conventional solution-based spin-coating, spray-drying and electrodeposition methods offer limited control over the film thickness and conformality, and are less feasible from the industry points of view. Here advanced gas-phase thin film techniques could offer clear benefits, being for example free from solvent impurities. The ALD technique in particular – known as the state-of-the-art gas-phase thin-film technology in conventional microelectronics – yields precisely thickness-controlled, conformal, and uniform coatings over large-area and complex substrate surfaces. The ALD technology is already well integrated with the silicon-based PV industry for the fabrication of metal oxide surface passivation layers [213,214], where it has proven its capability to fulfil the cost, throughput and performance criteria. Moreover, we already have the required well-behaving ALD processes available for a number of Ln-based thin films [215], including those with promising photoluminescence and upconversion properties. The ALD precursors employed are non-toxic and safe to handle, but naturally the lanthanides used as the UC activators in general are considered as critical raw materials, which should be taken into account considering their mass production for GW-scale PV factories. Despite the great prospects, efforts to integrate the ALD-grown UC films with actual PV cells have remained scarce. An exciting idea would be to develop a new ALD UC coating that could simultaneously work as the surface passivation layer.

CRediT authorship contribution statement

Amr Ghazy: Conceptualization, Visualization, Writing – original draft. **Muhammad Safdar:** Writing – review & editing. **Mika Lastusaari:** Writing – original draft. **Hele Savin:** Writing – original draft. **Maarit Karppinen:** Conceptualization, Supervision, Funding acquisition, Writing – original draft.

Declaration of competing interest

The authors declare that they have no known competing financial interests or personal relationships that could have appeared to influence the work reported in this paper.

Acknowledgements

Funding was received from the Academy of Finland (Profi 3), and the Flagship Programme, Photonics Research and Innovation (PREIN). Also, Amr Ghazy acknowledges Jenny & Antti Wihuri Foundation for financial support.

References

[1] Global market for solar power overview, Sol. Power Eur. (2020) 17. https://www.solarpowereurope.org/european-market-outlook-for-solar-power-2020-2024/. (Accessed 11 January 2021).
[2] A. Khare, A critical review on the efficiency improvement of upconversion assisted solar cells, J. Alloys Compd. 821 (2020) 153214, https://doi.org/10.1016/j.jallcom.2019.153214.
[3] K. Yoshikawa, H. Kawasaki, W. Yoshida, T. Irie, K. Konishi, K. Nakano, T. Uto, D. Adachi, M. Kanematsu, H. Uzu, K. Yamamoto, Silicon heterojunction solar cell with interdigitated back contacts for a photoconversion efficiency over 26%, Nat. Energy 2 (2017) 1–8, https://doi.org/10.1038/nenergy.2017.32.
[4] D.E. Carlson, C.R. Wronski, Amorphous silicon solar cell, Appl. Phys. Lett. 28 (1976) 671–673, https://doi.org/10.1063/1.88617.
[5] B. O'Regan, M. Grätzel, A low-cost, high-efficiency solar cell based on dye-sensitized colloidal TiO_2 films, Nature 353 (1991) 737–740, https://doi.org/10.1038/353737a0.
[6] A. Kojima, K. Teshima, Y. Shirai, T. Miyasaka, Organometal halide perovskites as visible-light sensitizers for photovoltaic cells, J. Am. Chem. Soc. 131 (2009) 6050–6051, https://doi.org/10.1021/ja809598r.
[7] N.G. Park, Perovskite solar cells: an emerging photovoltaic technology, Mater. Today 18 (2015) 65–72, https://doi.org/10.1016/j.mattod.2014.07.007.
[8] W.S. Yang, J.H. Noh, N.J. Jeon, Y.C. Kim, S. Ryu, J. Seo, S. Il Seok, High-performance photovoltaic perovskite layers fabricated through intramolecular exchange, Science 348 (80) (2015) 1234–1237, https://doi.org/10.1126/science.aaa9272.
[9] T. Trupke, M.A. Green, P. Würfel, Improving solar cell efficiencies by up-conversion of sub-band-gap light, J. Appl. Phys. 92 (2002) 4117–4122, https://doi.org/10.1063/1.1505677.
[10] J.C. Goldschmidt, S. Fischer, Upconversion for photovoltaics - a review of materials, devices and concepts for performance enhancement, Adv. Opt. Mater. 3 (2015) 510–535, https://doi.org/10.1002/adom.201500024.
[11] W. Shockley, H.J. Queisser, Detailed balance limit of efficiency of p-n junction solar cells, J. Appl. Phys. 32 (1961) 510–519, https://doi.org/10.1063/1.1736034.
[12] J. De Wild, A. Meijerink, J.K. Rath, W.G.J.H.M. Van Sark, R.E.I. Schropp, Upconverter solar cells: materials and applications, Energy Environ. Sci. 4 (2011) 4835–4848, https://doi.org/10.1039/c1ee01659h.
[13] J.F. Geisz, R.M. France, K.L. Schulte, M.A. Steiner, A.G. Norman, H.L. Guthrey, M. R. Young, T. Song, T. Moriarty, Six-junction III–V solar cells with 47.1% conversion efficiency under 143 Suns concentration, Nat. Energy 5 (2020) 326–335, https://doi.org/10.1038/s41560-020-0598-5.
[14] A. Al-Ashouri, E. Köhnen, B. Li, A. Magomedov, H. Hempel, P. Caprioglio, J. A. Márquez, A.B.M. Vilches, E. Kasparavicius, J.A. Smith, N. Phung, D. Menzel, M. Grischek, L. Kegelmann, D. Skroblin, C. Gollwitzer, T. Malinauskas, M. Jošt, G. Matič, B. Rech, R. Schlatmann, M. Topič, L. Korte, A. Abate, B. Stannowski, D. Neher, M. Stolterfoht, T. Unold, V. Getautis, S. Albrecht, Monolithic perovskite/silicon tandem solar cell with >29% efficiency by enhanced hole extraction, Science 370 (2020) 1300–1309, https://doi.org/10.1126/science.abd4016.
[15] E. Hemmer, A. Benayas, F. Légaré, F. Vetrone, Exploiting the biological windows: current perspectives on fluorescent bioprobes emitting above 1000 nm, Nanoscale Horizons 1 (2016) 168–184, https://doi.org/10.1039/c5nh00073d.
[16] J. Xu, P. Yang, M. Sun, H. Bi, B. Liu, D. Yang, S. Gai, F. He, J. Lin, Highly emissive dye-sensitized upconversion nanostructure for dual-photosensitizer photodynamic therapy and bioimaging, ACS Nano 11 (2017) 4133–4144, https://doi.org/10.1021/acsnano.7b00944.
[17] Z. Zhang, S. Shikha, J. Liu, J. Zhang, Q. Mei, Y. Zhang, Upconversion nanoprobes: recent advances in sensing applications, Anal. Chem. 91 (2019) 548–568, https://doi.org/10.1021/acs.analchem.8b04049.
[18] R. Deng, F. Qin, R. Chen, W. Huang, M. Hong, X. Liu, Temporal full-colour tuning through non-steady-state upconversion, Nat. Nanotechnol. 10 (2015) 237–242, https://doi.org/10.1038/nnano.2014.317.
[19] X. Huang, S. Han, W. Huang, X. Liu, Enhancing solar cell efficiency: the search for luminescent materials as spectral converters, Chem. Soc. Rev. 42 (2013) 173–201, https://doi.org/10.1039/C2CS35288E.
[20] P. Gibart, F. Auzel, J.C. Guillaume, K. Zahraman, Below band-gap IR response of substrate-free GaAs solar cells using two-photon up-conversion, Jpn. J. Appl. Phys., Part 1 (35) (1996) 4401–4402, https://doi.org/10.1143/jjap.35.4401.
[21] G.-B. Shan, G.P. Demopoulos, Near-infrared sunlight harvesting in dye-sensitized solar cells via the insertion of an upconverter-TiO_2 nanocomposite layer, Adv. Mater. 22 (2010) 4373–4377, https://doi.org/10.1002/adma.201001816.
[22] W. Wang, M. Zhao, C. Zhang, H. Qian, Recent advances in controlled synthesis of upconversion nanoparticles and semiconductor heterostructures, Chem. Rec. 20 (2020) 2–9, https://doi.org/10.1002/tcr.201900006.
[23] Y. Wang, K. Zheng, S. Song, D. Fan, H. Zhang, X. Liu, Remote manipulation of upconversion luminescence, Chem. Soc. Rev. 47 (2018) 6473–6485, https://doi.org/10.1039/c8cs00124c.
[24] D. Li, H. Ågren, G. Chen, Near infrared harvesting dye-sensitized solar cells enabled by rare-earth upconversion materials, Dalton Trans. 47 (2018) 8526–8537, https://doi.org/10.1039/C7DT04461E.
[25] S.K. Karunakaran, G.M. Arumugam, W. Yang, S. Ge, S.N. Khan, X. Lin, G. Yang, Research progress on the application of lanthanide-ion-doped phosphor materials in perovskite solar cells, ACS Sustain. Chem. Eng. 9 (2021) 1035–1060, https://doi.org/10.1021/acssuschemeng.0c07319.
[26] F. Auzel, Upconversion and anti-Stokes processes with f and d Ions in solids, Chem. Rev. 104 (2004) 139–173, https://doi.org/10.1021/cr020357g.
[27] T.N. Singh-Rachford, F.N. Castellano, Photon upconversion based on sensitized triplet-triplet annihilation, Coord. Chem. Rev. 254 (2010) 2560–2573, https://doi.org/10.1016/j.ccr.2010.01.003.
[28] S.V. Eliseeva, Luminescence of lanthanide ions in coordination compounds and nanomaterials, in: Ana de Bettencourt-Dias (Ed.), Wiley, 2015, https://doi.org/10.1002/anie.201504040.
[29] J. Zhou, Q. Liu, W. Feng, Y. Sun, F. Li, Upconversion luminescent materials: advances and applications, Chem. Rev. 115 (2015) 395–465, https://doi.org/10.1021/cr400478f.
[30] H. Dong, L.D. Sun, C.H. Yan, Energy transfer in lanthanide upconversion studies for extended optical applications, Chem. Soc. Rev. 44 (2015) 1608–1634, https://doi.org/10.1039/c4cs00188e.
[31] F. Huang, X. Liu, Y. Ma, S. Kang, L. Hu, D. Chen, Origin of near to middle infrared luminescence and energy transfer process of Er^{3+}/Yb^{3+} co-doped fluorotellurite glasses under different excitations, Sci. Rep. 5 (2015) 8233, https://doi.org/10.1038/srep08233.
[32] M. Safdar, A. Ghazy, M. Lastusaari, M. Karppinen, Lanthanide-based inorganic-organic hybrid materials for photon-upconversion, J. Mater. Chem. C. 8 (2020) 6946–6965, https://doi.org/10.1039/d0tc01216e.
[33] Y. Arai, T. Yamashidta, T. Suzuki, Y. Ohishi, Upconversion properties of Tb^{3+}-Yb^{3+} codoped fluorophosphate glasses, J. Appl. Phys. 105 (2009), 083105, https://doi.org/10.1063/1.3112010.
[34] S.V. Eliseeva, J.C.G. Bünzli, Lanthanide luminescence for functional materials and bio-sciences, Chem. Soc. Rev. 39 (2010) 189–227, https://doi.org/10.1039/b905604c.
[35] F.E. Auzel, Materials and devices using double-pumped phosphors with energy transfer, Proc. IEEE 61 (1973) 758–786, https://doi.org/10.1109/PROC.1973.9155.
[36] A. Nadort, J. Zhao, E.M. Goldys, Lanthanide upconversion luminescence at the nanoscale: Fundamentals and optical properties, Nanoscale 8 (2016) 13099–13130, https://doi.org/10.1039/c5nr08477f.
[37] F. Wang, X. Liu, Recent advances in the chemistry of lanthanide-doped upconversion nanocrystals, Chem. Soc. Rev. 38 (2009) 976–989, https://doi.org/10.1039/b809132n.
[38] F. Auzel, D. Pecile, Comparison and efficiency of materials for summation of photons assisted by energy transfer, J. Lumin. 8 (1973) 32–43, https://doi.org/10.1016/0022-2313(73)90033-1.
[39] N. Menyuk, K. Dwight, J.W. Pierce, $NaYF_4$:Yb,Er - an efficient upconversion phosphor, Appl. Phys. Lett. 21 (1972) 159–161, https://doi.org/10.1063/1.1654325.
[40] T. Kano, H. Yamamoto, Y. Otomo, $NaLnF_4$:Yb^{3+},Er^{3+} (Ln:Y,Gd,La): efficient green-emitting infrared-excited phosphors, J. Electrochem. Soc. 119 (1972) 1561, https://doi.org/10.1149/1.2404042.
[41] K.W. Krämer, D. Biner, G. Frei, H.U. Güdel, M.P. Hehlen, S.R. Lüthi, Hexagonal sodium yttrium fluoride based green and blue emitting upconversion phosphors, Chem. Mater. 16 (2004) 1244–1251, https://doi.org/10.1021/cm031124o.
[42] D. Kumar, S.K. Sharma, S. Verma, V. Sharma, V. Kumar, A short review on rare earth doped $NaYF_4$ upconverted nanomaterials for solar cell applications. Mater. Today Proc., Elsevier Ltd, 2020, pp. 1868–1874, https://doi.org/10.1016/j.matpr.2020.01.243.
[43] F. Wang, J. Wang, X. Liu, Direct evidence of a surface quenching effect on size-dependent luminescence of upconversion nanoparticles, Angew. Chem. Int. Ed. 49 (2010) 7456–7460, https://doi.org/10.1002/anie.201003959.
[44] H. Lakhotiya, A. Nazir, S. Roesgaard, E. Eriksen, J. Christiansen, M. Bondesgaard, F.C.J.M. Van Veggel, B.B. Iversen, P. Balling, B. Julsgaard, Resonant plasmon-enhanced upconversion in monolayers of core-shell nanocrystals: role of shell

thickness, ACS Appl. Mater. Interfaces 11 (2019) 1209–1218, https://doi.org/10.1021/acsami.8b15564.
[45] F. Trabelsi, F. Mercier, E. Blanquet, A. Crisci, R. Salhi, Synthesis of upconversion TiO_2:Er^{3+}-Yb^{3+} nanoparticles and deposition of thin films by spin coating technique, Ceram. Int. 46 (2020) 28183–28192, https://doi.org/10.1016/j.ceramint.2020.07.317.
[46] H.J. da Silva, J.P. Batista, L.A. Rocha, E.J. Nassar, Improved efficiency of silicon polycrystalline commercial photovoltaic cells coated with a co-doped Er^{3+}/Yb^{3+} silica matrix, J. Mater. Sci. Mater. Electron. 30 (2019) 16886–16891, https://doi.org/10.1007/s10854-019-01549-w.
[47] S. George, Atomic layer deposition: an overview, Chem. Rev. 110 (2010) 111–131.
[48] M. Tuomisto, Z. Giedraityte, M. Karppinen, M. Lastusaari, Photon up-converting $(Yb,Er)_2O_3$ thin films by atomic layer deposition, Phys. Status Solidi Rapid Res. Lett. 11 (2017) 1700076, https://doi.org/10.1002/pssr.201700076.
[49] A. Ghazy, M. Safdar, M. Lastusaari, A. Aho, A. Tukiainen, H. Savin, M. Guina, M. Karppinen, Luminescent $(Er,Ho)_2O_3$ thin films by ALD to enhance the performance of silicon solar cells, Sol. Energy Mater. Sol. Cells 219 (2021) 110787, https://doi.org/10.1016/j.solmat.2020.110787.
[50] C. de Mayrinck, R.L. Siqueira, J. Esbenshade, M.A. Schiavon, R.C. de Lima, H. P. Barbosa, S.J. Lima Ribeiro, J.L. Ferrari, Downconversion and upconversion observed from Er^{3+}/Yb^{3+}/Eu^{3+} tri-doped-Y_2O_3 for application in energy conversion, J. Alloys Compd. 816 (2020) 152591, https://doi.org/10.1016/j.jallcom.2019.152591.
[51] H. Wu, Z. Hao, L. Zhang, X. Zhang, G.-H. Pan, Y. Luo, H. Wu, H. Zhao, H. Zhang, J. Zhang, Enhancing IR to NIR upconversion emission in Er^{3+}-sensitized phosphors by adding Yb^{3+} as a highly efficient NIR-emitting center for photovoltaic applications, CrystEngComm 22 (2020) 229–236, https://doi.org/10.1039/C9CE01386E.
[52] K.K. Markose, R. Anjana, A. Antony, M.K. Jayaraj, Synthesis of Yb^{3+}/Er^{3+} co-doped Y_2O_3, YOF and YF_3 UC phosphors and their application in solar cell for sub-bandgap photon harvesting, J. Lumin. 204 (2018) 448–456, https://doi.org/10.1016/j.jlumin.2018.08.005.
[53] P. Głuchowski, Ł. Marciniak, M. Lastusaari, W. Stręk, Key factors tuning upconversion and near infrared luminescence in nanosized Lu_2O_3:Er^{3+},Yb^{3+}, J. Alloys Compd. 799 (2019) 481–494, https://doi.org/10.1016/j.jallcom.2019.05.358.
[54] H. Shaier, A. Salah, W.M. Mousa, S.S. Hamed, I.K. Battisha, Physical properties and up-conversion development of Ho^{3+}ions loaded in nano-composite silica titania thin film, Mater. Res. Express 7 (2020), 096403, https://doi.org/10.1088/2053-1591/abb4fe.
[55] J.M.M. Buarque, D. Manzani, S.L. Scarpari, M. Nalin, S.J.L. Ribeiro, J. Esbenshade, M.A. Schiavon, J.L. Ferrari, SiO_2-TiO_2 doped with Er^{3+}/Yb^{3+}/Eu^{3+} photoluminescent material: a spectroscopy and structural study about potential application for improvement of the efficiency on solar cells, Mater. Res. Bull. 107 (2018) 295–307, https://doi.org/10.1016/j.materresbull.2018.07.007.
[56] J. Zhao, J. Li, Y. Wang, W. Ni, Fabrication and broadband upconversion luminescence of Au@TiO_2:Yb,Er core-shell nanostructures, Chem. Lett. 48 (2019) 651–653, https://doi.org/10.1246/cl.190184.
[57] R.Y.S. Zampiva, C.G. Kaufmann, L.H. Acauan, R.L. Seeger, F. Bonatto, C. D. Boeira, W.Q. Santos, C. Jacinto, C.A. Figueroa, L.S. Dorneles, A.K. Alves, C. P. Bergmann, C.S. ten Caten, Luminescent anti-reflection coatings based on Er^{3+} doped forsterite for commercial silicon solar cells applications, Sol. Energy 170 (2018) 752–761, https://doi.org/10.1016/j.solener.2018.05.097.
[58] J. Zhang, J. Chen, F. Qian, Y. Zhang, S, An, Ratiometric fluorescence temperature-sensing properties of Eu^{3+} and Tm^{3+} in $Gd_{4.67}Si_3O_{13}$ oxide host, Opt Laser. Technol. 138 (2021) 106854, https://doi.org/10.1016/j.optlastec.2020.106854.
[59] J. Zhang, J. Chen, Y. Zhang, S. An, Yb^{3+}/Tm^{3+} and Yb^{3+}/Ho^{3+} doped $NaY_9(SiO_4)_6O_2$ phosphors: upconversion luminescence processes, temperature-dependent emission spectra and optical temperature-sensing properties, J. Alloys Compd. 860 (2021) 158473, https://doi.org/10.1016/j.jallcom.2020.158473.
[60] V. Kumar, A. Pandey, S.K. Swami, O.M. Ntwaeaborwa, H.C. Swart, V. Dutta, Synthesis and characterization of Er^{3+}-Yb^{3+} doped ZnO upconversion nanoparticles for solar cell application, J. Alloys Compd. 766 (2018) 429–435, https://doi.org/10.1016/j.jallcom.2018.07.012.
[61] M.S. Morassaei, A. Salehabadi, A. Akbari, S.H. Tavassoli, M. Salavati-Niasari, Enhanced dye sensitized solar cells efficiency by utilization of an external layer of $CaCe_2(MoO_4)_4$:Er^{3+}/Yb^{3+} nanoparticles, J. Alloys Compd. 769 (2018) 732–739, https://doi.org/10.1016/j.jallcom.2018.08.037.
[62] P.K. Vishwakarma, S.B. Rai, A. Bahadur, Intense red and green emissions from Ho^{3+}/Yb^{3+} co-doped sodium gadolinium molybdate nano-phosphor: effect of calcination temperature and Intrinsic optical bistability, Mater. Res. Bull. 133 (2021) 111041, https://doi.org/10.1016/j.materresbull.2020.111041.
[63] W. Ge, W. Gao, Y. Tian, P. Zhang, J. Zhu, Y. Li, Tunable dual-mode photoluminescences from $SrAl_2O_4$: Eu/Yb nanofibers by different atmospheric annealing, J. Alloys Compd. 859 (2021) 158261, https://doi.org/10.1016/j.jallcom.2020.158261.
[64] J. Xu, Y. Zhou, Z. Li, C. Lin, X. Zheng, T. Lin, X. Wu, F. Wang, Microstructural, ferroelectric and photoluminescence properties of Er^{3+}-doped $Ba_{0.85}Ca_{0.15}Ti_{0.9}Zr_{0.1}O_3$ thin films, Mater. Chem. Phys. 262 (2021) 124320, https://doi.org/10.1016/j.matchemphys.2021.124320.
[65] O.B. Silva, V.A.G. Rivera, Y. Ledemi, Y. Messaddeq, E. Marega, Germanium concentration effects on the visible emission properties of Er^{3+} in tellurite glasses, J. Lumin. 232 (2021) 117808, https://doi.org/10.1016/j.jlumin.2020.117808.
[66] A. Kumar, A. Bahadur, Intense green upconversion emission by photon avalanche process from Er^{3+}/Yb^{3+} co-doped $NaBi(WO_4)_2$ phosphor, J. Alloys Compd. 857 (2021) 158196, https://doi.org/10.1016/j.jallcom.2020.158196.
[67] I. Norrbo, I. Hyppänen, M. Lastusaari, Up-conversion luminescence – a new property in tenebrescent and persistent luminescent hackmanites, J. Lumin. 191 (2017) 28–34, https://doi.org/10.1016/j.jlumin.2017.02.046.
[68] Y. Zhang, H. Lei, G. Li, L. Zeng, J. Tang, Yb^{3+}/Er^{3+} co-doped transparent tellurite glass-ceramic for enhanced upconversion luminescence, Opt. Mater. 99 (2020) 109552, https://doi.org/10.1016/j.optmat.2019.109552.
[69] M. Gunaseelan, S. Yamini, G.A. Kumar, J. Senthilselvan, Highly efficient upconversion luminescence in hexagonal $NaYF_4$:Yb^{3+},Er^{3+} nanocrystals synthesized by a novel reverse microemulsion method, Opt. Mater. 75 (2018) 174–186, https://doi.org/10.1016/j.optmat.2017.10.012.
[70] A.L. Pellegrino, M.R. Catalano, P. Cortelletti, G. Lucchini, A. Speghini, G. Malandrino, Novel sol-gel fabrication of Yb^{3+}/Tm^{3+} co-doped β-$NaYF_4$ thin films and investigation of their upconversion properties, Photochem. Photobiol. Sci. 17 (2018) 1239–1246, https://doi.org/10.1039/c8pp00295a.
[71] F. Xu, H. Gao, J. Liang, S. Jin, J. Zhao, Y. Liu, H. Zhang, Z. Zhang, Y. Mao, Enhanced upconversion luminescence in $Cu_{1.8}S$@$NaYF_4$:Yb@$NaYF_4$:Yb,Er core-shell nanoparticles, Ceram. Int. 45 (2019) 21557–21563, https://doi.org/10.1016/j.ceramint.2019.07.149.
[72] N. Ojha, M. Tuomisto, M. Lastusaari, L. Petit, Upconversion from fluorophosphate glasses prepared with $NaYF_4$:Er^{3+},Yb^{3+} nanocrystals, RSC Adv. 8 (2018), https://doi.org/10.1039/c8ra03298j, 19226–19236.
[73] X. Deng, C. Zhang, J. Zheng, X. Zhou, M. Yu, X. Chen, S. Huang, Highly bright Li(Gd,Y)F_4:Yb,Er upconverting nanocrystals incorporated hole transport layer for efficient perovskite solar cells, Appl. Surf. Sci. 485 (2019) 332–341, https://doi.org/10.1016/j.apsusc.2019.04.226.
[74] M. Gupta, M. Adnan, R. Nagarajan, G. Vijaya Prakash, Color-tunable upconversion in Er^{3+}/Yb^{3+}-codoped $KLaF_4$ nanophosphors by incorporation of Tm^{3+} ions for biological applications, ACS Omega 4 (2019) 2275–2282, https://doi.org/10.1021/acsomega.8b03075.
[75] M. Zeng, S. Singh, Z. Hens, J. Liu, F. Artizzu, R. Van Deun, Strong upconversion emission in $CsPbBr_3$ perovskite quantum dots through efficient $BaYF_5$:Yb,Ln sensitization, J. Mater. Chem. C 7 (2019) 2014–2021, https://doi.org/10.1039/c8tc06063k.
[76] H.K. Dan, T.D. Tap, H.X. Vinh, H.T. Nguyen-Truong, J. Qiu, D. Zhou, N.M. Ty, Effects of La^{3+} on the enhancement NIR quantum cutting and UC emissions in Nd^{3+}–Yb^{3+} co-doped transparent silicate glass-ceramics for solar cells, Opt. Mater. 95 (2019) 109229, https://doi.org/10.1016/j.optmat.2019.109229.
[77] Y. Li, Z. Di, J. Gao, P. Cheng, C. Di, G. Zhang, B. Liu, X. Shi, L.-D. Sun, L. Li, C.-H. Yan, Heterodimers made of upconversion nanoparticles and metal–organic frameworks, J. Am. Chem. Soc. 139 (2017) 13804–13810, https://doi.org/10.1021/jacs.7b07302.
[78] T. Wu, B. Li, J. Sun, M. Shao, X. Ma, Z. Bai, Preparation of PbF_2:Ho^{3+},Er^{3+},Yb^{3+} phosphors and its multi-wavelength sensitive upconversion luminescence mechanism, Mater. Res. Bull. 107 (2018) 308–313, https://doi.org/10.1016/j.materresbull.2018.08.006.
[79] A.L. Pellegrino, P. Cortelletti, M. Pedroni, A. Speghini, G. Malandrino, Nanostructured CaF_2:Ln^{3+} (Ln^{3+} = Yb^{3+}/Er^{3+}, Yb^{3+}/Tm^{3+}) thin films: MOCVD fabrication and their upconversion properties, Adv. Mater. Interfaces 4 (2017) 1700245, https://doi.org/10.1002/admi.201700245.
[80] A.L. Pellegrino, S. La Manna, A. Bartasyte, P. Cortelletti, G. Lucchini, A. Speghini, G. Malandrino, Upconverting tri-doped calcium fluoride-based thin films: a comparison of the MOCVD and sol-gel preparation methods, J. Mater. Chem. C 8 (2020) 3865–3877, https://doi.org/10.1039/c9tc06350a.
[81] T. Castro, D. Manzani, S.J.L. Ribeiro, Up-conversion mechanisms in Er^{3+}-doped fluoroindate glasses under 1550 nm excitation for enhancing photocurrent of crystalline silicon solar cell, J. Lumin. 200 (2018) 260–264, https://doi.org/10.1016/j.jlumin.2018.04.028.
[82] A. Tymiński, T. Grzyb, Are rare earth phosphates suitable as hosts for upconversion luminescence? Studies on nanocrystalline $REPO_4$ (RE=Y, La, Gd, Lu) doped with Yb^{3+} and Eu^{3+}, Tb^{3+}, Ho^{3+}, Er^{3+} or Tm^{3+} ions, J. Lumin. 181 (2017) 411–420, https://doi.org/10.1016/j.jlumin.2016.09.028.
[83] B. Glorieux, T. Salminen, J. Massera, M. Lastusaari, L. Petit, Better understanding of the role of SiO_2, P_2O_5 and Al_2O_3 on the spectroscopic properties of Yb^{3+} doped silica sol-gel glasses, J. Non-Cryst. Solids 482 (2018) 46–51, https://doi.org/10.1016/j.jnoncrysol.2017.12.021.
[84] M. Lun, W. Wu, Z. Xing, H. Song, Y. Wang, W. Li, B. Chu, Q. He, Upconversion photoluminescence of Er^{3+} and Yb^{3+} codoped MoS_2 powders, J. Lumin. 223 (2020) 117189, https://doi.org/10.1016/j.jlumin.2020.117189.
[85] Z. Giedraityte, M. Tuomisto, M. Lastusaari, M. Karppinen, Three- and two-photon NIR-to-vis (Yb,Er) upconversion from ALD/MLD-fabricated molecular hybrid thin films, ACS Appl. Mater. Interfaces 10 (2018) 8845–8852, https://doi.org/10.1021/acsami.7b19303.
[86] M. Tuomisto, Z. Giedraityte, L. Mai, A. Devi, V. Boiko, K. Grzeszkiewicz, D. Hreniak, M. Karppinen, M. Lastusaari, Up-converting ALD/MLD thin films with Yb^{3+}, Er^{3+} in amorphous organic framework, J. Lumin. 213 (2019) 310–315, https://doi.org/10.1016/j.jlumin.2019.05.028.
[87] J. Dutta, V.K. Rai, M.M. Durai, R. Thangavel, Development of Y_2O_3:Ho^{3+}/Yb^{3+} upconverting nanophosphors for enhancing solar cell efficiency of dye-sensitized solar cells, IEEE J. Photovoltaics 9 (2019) 1040–1045, https://doi.org/10.1109/JPHOTOV.2019.2912719.
[88] H. Li, C. Chen, J. Jin, W. Bi, B. Zhang, X. Chen, L. Xu, D. Liu, Q. Dai, H. Song, Near-infrared and ultraviolet to visible photon conversion for full spectrum

response perovskite solar cells, Nanomater. Energy 50 (2018) 699–709, https://doi.org/10.1016/j.nanoen.2018.06.024.
[89] H. Huang, C. Modanese, S. Sun, G. von Gastrow, J. Wang, T.P. Pasanen, S. Li, L. Wang, Y. Bao, Z. Zhu, S. Sneck, H. Savin, Effective passivation of p+ and n+ emitters using $SiO_2/Al_2O_3/SiN_x$ stacks: surface passivation mechanisms and application to industrial p-PERT bifacial Si solar cells, Sol. Energy Mater. Sol. Cells 186 (2018) 356–364, https://doi.org/10.1016/j.solmat.2018.07.007.
[90] H. Huang, L. Wang, L. Mandrell, C. Modanese, S. Sun, J. Wang, A. Wang, J. Zhao, B. Adibi, H. Savin, Boron implanted junction with in situ oxide passivation and application to p-PERT bifacial silicon solar cell, Phys. Status Solidi Appl. Mater. Sci. 216 (2019) 1800414, https://doi.org/10.1002/pssa.201800414.
[91] K. Chen, V. Vahanissi, Z.J. Rad, J.P. Lehtio, P. Laukkanen, M. Yli-Koski, H. Savin, Black Silicon Boron Emitter Solar Cells with EQE above 95% in UV, in: Conf. Rec. IEEE Photovolt. Spec. Conf., Institute of Electrical and Electronics Engineers Inc., 2020, pp. 2586–2589, https://doi.org/10.1109/PVSC45281.2020.9300686.
[92] H. Savin, P. Repo, G. Von Gastrow, P. Ortega, E. Calle, M. Garín, R. Alcubilla, Black silicon solar cells with interdigitated back-contacts achieve 22.1% efficiency, Nat. Nanotechnol. 10 (2015) 624–628, https://doi.org/10.1038/nnano.2015.89.
[93] M. Saboktakin, X. Ye, S.J. Oh, S.H. Hong, A.T. Fafarman, U.K. Chettiar, N. Engheta, C.B. Murray, C.R. Kagan, Metal-enhanced upconversion luminescence tunable through metal nanoparticle-nanophosphor separation, ACS Nano 6 (2012) 8758–8766, https://doi.org/10.1021/nn302466r.
[94] J. Wang, Y. Niu, M. Hojamberdiev, F.M. Alamgir, Y. Cai, K. Jacob, Novel triple-layered photoanodes based on TiO_2 nanoparticles, TiO_2 nanotubes, and β-$NaYF_4$:Er^{3+},Yb^{3+}@SiO_2@TiO_2 for highly efficient dye-sensitized solar cells, Sol. Energy Mater. Sol. Cells 160 (2017) 361–371, https://doi.org/10.1016/j.solmat.2016.10.046.
[95] E. Ahvenniemi, M. Karppinen, In situ atomic/molecular layer-by-layer deposition of inorganic-organic coordination network thin films from gaseous precursors, Chem. Mater. 28 (2016) 6260–6265, https://doi.org/10.1021/acs.chemmater.6b02496.
[96] J. Penttinen, M. Nisula, M. Karppinen, New s-block metal pyridinedicarboxylate network structures through gas-phase thin-film synthesis, Chem. Eur J. 25 (2019) 11466–11473, https://doi.org/10.1002/chem.201901034.
[97] P.A. Hansen, H. Fjellvåg, T.G. Finstad, O. Nilsen, Luminescence properties of europium titanate thin films grown by atomic layer deposition, RSC Adv. 4 (2014) 11876–11883, https://doi.org/10.1039/c3ra47469k.
[98] Z. Giedraityte, P. Sundberg, M. Karppinen, Flexible inorganic–organic thin film phosphors by ALD/MLD, J. Mater. Chem. C 3 (2015) 12316–12321, https://doi.org/10.1039/C5TC03201F.
[99] Z. Giedraityte, L.S. Johansson, M. Karppinen, ALD/MLD fabrication of luminescent Eu-organic hybrid thin films using different aromatic carboxylic acid components with N and O donors, RSC Adv. 6 (2016) 103412–103417, https://doi.org/10.1039/c6ra24175a.
[100] L. Mai, Z. Giedraityte, M. Schmidt, D. Rogalla, S. Scholz, A.D. Wieck, A. Devi, M. Karppinen, Atomic/molecular layer deposition of hybrid inorganic–organic thin films from erbium guanidinate precursor, J. Mater. Sci. 52 (2017) 6216–6224, https://doi.org/10.1007/s10853-017-0855-6.
[101] M.N. Getz, P.A. Hansen, Ø.S. Fjellvåg, M.A.K. Ahmed, H. Fjellvåg, O. Nilsen, Intense NIR emission in YVO_4:Yb^{3+} thin films by atomic layer deposition, J. Mater. Chem. C 5 (2017) 8572–8578, https://doi.org/10.1039/c7tc02135f.
[102] M. Getz, P.A. Hansen, M.A.K. Ahmed, H. Fjellvåg, O. Nilsen, Luminescent $YbVO_4$ by atomic layer deposition, Dalton Trans. 46 (2017) 3008–3013, https://doi.org/10.1039/c7dt00253j.
[103] P.-A. Hansen, H. Fjellvåg, T.G. Finstad, O. Nilsen, Luminescence properties of lanthanide and ytterbium lanthanide titanate thin films grown by atomic layer deposition, J. Vac. Sci. Technol., A 34 (2015), 01A130, https://doi.org/10.1116/1.4936389.
[104] V. Kiisk, A. Tamm, K. Utt, J. Kozlova, H. Mändar, L. Puust, J. Aarik, I. Sildos, Photoluminescence of atomic layer deposited ZrO_2:Dy^{3+} thin films, Thin Solid Films 583 (2015) 70–75, https://doi.org/10.1016/j.tsf.2015.03.041.
[105] M. Safdar, A. Ghazy, M. Tuomisto, M. Lastusaari, M. Karppinen, Effect of carbon backbone on luminescence properties of Eu-organic hybrid thin films prepared by ALD/MLD, J. Mater. Sci. 56 (2021) 12634–12642, https://doi.org/10.1007/s10853-021-06094-8.
[106] M.A. Hernández-Rodríguez, M.H. Imanieh, L.L. Martín, I.R. Martín, Experimental enhancement of the photocurrent in a solar cell using upconversion process in fluoroindate glasses exciting at 1480 nm, Sol. Energy Mater. Sol. Cells 116 (2013) 171–175, https://doi.org/10.1016/j.solmat.2013.04.023.
[107] M. Rüdiger, S. Fischer, J. Frank, A. Ivaturi, B.S. Richards, K.W. Krämer, M. Hermle, J.C. Goldschmidt, Bifacial n-type silicon solar cells for upconversion applications, Sol. Energy Mater. Sol. Cells 128 (2014) 57–68, https://doi.org/10.1016/j.solmat.2014.05.014.
[108] S. Fischer, E. Favilla, M. Tonelli, J.C. Goldschmidt, Record efficient upconverter solar cell devices with optimized bifacial silicon solar cells and monocrystalline BaY_2F_8:30% Er^{3+} upconverter, Sol. Energy Mater. Sol. Cells 136 (2015) 127–134, https://doi.org/10.1016/j.solmat.2014.12.023.
[109] A. Boccolini, R. Faoro, E. Favilla, S. Veronesi, M. Tonelli, BaY_2F_8 doped with Er^{3+}: An upconverter material for photovoltaic application, J. Appl. Phys. 114 (2013), 064904, https://doi.org/10.1063/1.4817171.
[110] A. Shalav, B.S. Richards, T. Trupke, K.W. Krämer, H.U. Güdel, Application of $NaYF_4$:Er^{3+} up-converting phosphors for enhanced near-infrared silicon solar cell response, Appl. Phys. Lett. 86 (2005), 013505, https://doi.org/10.1063/1.1844592.
[111] T. Trupke, A. Shalav, B.S. Richards, P. Würfel, M.A. Green, Efficiency enhancement of solar cells by luminescent up-conversion of sunlight, Sol. Energy Mater. Sol. Cells 90 (2006) 3327–3338, https://doi.org/10.1016/j.solmat.2005.09.021.
[112] J. de Wild, A. Meijerink, J.K. Rath, W.G.J.H.M. van Sark, R.E.I. Schropp, Towards upconversion for amorphous silicon solar cells, Sol. Energy Mater. Sol. Cells 94 (2010) 1919–1922, https://doi.org/10.1016/j.solmat.2010.06.006.
[113] J. De Wild, J.K. Rath, A. Meijerink, W.G.J.H.M. Van Sark, R.E.I. Schropp, Enhanced near-infrared response of a-Si:H solar cells with β-$NaYF_4$:Yb^{3+} (18%), Er^{3+} (2%) upconversion phosphors, Sol. Energy Mater. Sol. Cells 94 (2010) 2395–2398, https://doi.org/10.1016/j.solmat.2010.08.024.
[114] X.D. Zhang, X. Jin, D.F. Wang, S.Z. Xiong, X.H. Geng, Y. Zhao, Synthesis of $NaYF_4$: Yb, Er nanocrystals and its application in silicon thin film solar cells, Phys. Status Solidi 7 (2010) 1128–1131, https://doi.org/10.1002/pssc.200982762.
[115] Y. Chen, W. He, Y. Jiao, H. Wang, X. Hao, J. Lu, S.E. Yang, β-$NaYF_4$:Er^{3+} (10%) microprisms for the enhancement of a-Si:H solar cell near-infrared responses, J. Lumin. 132 (2012) 2247–2250, https://doi.org/10.1016/j.jlumin.2012.04.011.
[116] D. Liu, Q. Wang, Q. Wang, Near-infrared light harvesting of upconverting $NaYF_4$: Yb^{3+}/Er^{3+} -based amorphous silicon solar cells investigated by an optical filter, Beilstein J. Nanotechnol. 9 (2018) 2788–2793, https://doi.org/10.3762/bjnano.9.260.
[117] X. Cheng, H. Ge, Y. Wei, K. Zhang, W. Su, J. Zhou, L. Yin, Q. Zhan, S. Jing, L. Huang, Design for brighter photon upconversion emissions via energy level overlap of lanthanide ions, ACS Nano 12 (2018) 10992–10999, https://doi.org/10.1021/acsnano.8b04988.
[118] F. Lahoz, C. Pérez-Rodríguez, S.E. Hernández, I.R. Martín, V. Lavín, U. R. Rodríguez-Mendoza, Upconversion mechanisms in rare-earth doped glasses to improve the efficiency of silicon solar cells, Sol. Energy Mater. Sol. Cells 95 (2011) 1671–1677, https://doi.org/10.1016/j.solmat.2011.01.027.
[119] K.V. Krishnaiah, P. Venkatalakshmamma, C. Basavapoornima, I.R. Martín, K. Soler-Carracedo, M.A. Hernández-Rodríguez, V. Venkatramu, C.K. Jayasankar, Er^{3+}-doped tellurite glasses for enhancing a solar cell photocurrent through photon upconversion upon 1500 nm excitation, Mater. Chem. Phys. 199 (2017) 67–72, https://doi.org/10.1016/j.matchemphys.2017.06.003.
[120] K. Kakiage, Y. Aoyama, T. Yano, K. Oya, J.I. Fujisawa, M. Hanaya, Highly-efficient dye-sensitized solar cells with collaborative sensitization by silyl-anchor and carboxy-anchor dyes, Chem. Commun. 51 (2015) 15894–15897, https://doi.org/10.1039/c5cc06759f.
[121] R. Qin, X. Jinhua, J. Hu, L. Zhao, Effect of luminescent material $NaYbF_4$:Ho^{3+} on the photovoltaic performance of dye-sensitized solar cells, J. Mater. Sci. Mater. Electron. 32 (2021) 1445–1456, https://doi.org/10.1007/s10854-020-04915-1.
[122] P. Ramasamy, J. Kim, Combined plasmonic and upconversion rear reflectors for efficient dye-sensitized solar cells, Chem. Commun. 50 (2014) 879–881, https://doi.org/10.1039/C3CC47290F.
[123] L. Li, Y. Yang, R. Fan, S. Chen, P. Wang, B. Yang, W. Cao, Conductive upconversion Er,Yb-FTO nanoparticle coating to replace Pt as a low-cost and high-performance counter electrode for dye-sensitized solar cells, ACS Appl. Mater. Interfaces 6 (2014) 8223–8229, https://doi.org/10.1021/am5009776.
[124] M. Liu, Y. Lu, Z.B. Xie, G.M. Chow, Enhancing near-infrared solar cell response using upconverting transparent ceramics, Sol. Energy Mater. Sol. Cells 95 (2011) 800–803, https://doi.org/10.1016/j.solmat.2010.09.018.
[125] J. Bai, P. Duan, X. Wang, G. Han, M. Wang, G. Diao, Upconversion luminescence enhancement by Fe^{3+} doping in CeO_2:Yb/Er nanomaterials and their application in dye-sensitized solar cells, RSC Adv. 10 (2020) 18868–18874, https://doi.org/10.1039/D0RA02308F.
[126] M. Ambapuram, G. Maddala, N.B. Simhachalam, S. Sripada, S. Kalvapalli, V. S. Yerva Pedda, R. Mitty, Highly effective SnS composite counter electrode sandwiched bi-function CeO_2:Er^{3+}/Yb^{3+} assisted surface modified photoelectroded dye sensitized solar cell exceeds 9.5% efficiency, Sol. Energy 207 (2020) 1158–1164, https://doi.org/10.1016/j.solener.2020.07.030.
[127] Y. Qiao, S. Li, W. Liu, M. Ran, H. Lu, Y. Yang, Recent advances of rare-earth ion doped luminescent nanomaterials in perovskite solar cells, Nanomaterials 8 (2018) 43, https://doi.org/10.3390/nano8010043.
[128] T. Baikie, Y. Fang, J.M. Kadro, M. Schreyer, F. Wei, S.G. Mhaisalkar, M. Graetzel, T.J. White, Synthesis and crystal chemistry of the hybrid perovskite (CH_3NH_3) PbI_3 for solid-state sensitised solar cell applications, J. Mater. Chem. 1 (2013) 5628–5641, https://doi.org/10.1039/c3ta10518k.
[129] X. Chen, W. Xu, H. Song, C. Chen, H. Xia, Y. Zhu, D. Zhou, S. Cui, Q. Dai, J. Zhang, Highly efficient $LiYF_4$:Yb^{3+},Er^{3+} upconversion single crystal under solar cell spectrum excitation and photovoltaic application, ACS Appl. Mater. Interfaces 8 (2016) 9071–9079, https://doi.org/10.1021/acsami.5b12528.
[130] M. Schoenauer Sebag, Z. Hu, K. de Oliveira Lima, H. Xiang, P. Gredin, M. Mortier, L. Billot, L. Aigouy, Z. Chen, Microscopic evidence of upconversion-induced near-infrared light harvest in hybrid perovskite solar cells, ACS Appl. Energy Mater. 1 (2018) 3537–3543, https://doi.org/10.1021/acsaem.8b00518.
[131] F.-L. Meng, J.-J. Wu, E.-F. Zhao, Y.-Z. Zheng, M.-L. Huang, L.-M. Dai, X. Tao, J.-F. Chen, High-efficiency near-infrared enabled planar perovskite solar cells by embedding upconversion nanocrystals, Nanoscale 9 (2017) 18535–18545, https://doi.org/10.1039/C7NR05416E.
[132] M. He, X. Pang, X. Liu, B. Jiang, Y. He, H. Snaith, Z. Lin, Monodisperse dual-functional upconversion nanoparticles enabled near-infrared organolead halide perovskite solar cells, Angew. Chem. Int. Ed. 55 (2016) 4280–4284, https://doi.org/10.1002/anie.201600702.
[133] F. Yang, C. Liu, D. Wei, Y. Chen, J. Lu, S.E. Yang, Er^{3+}-Yb^{3+} co-doped TeO_2-PbF_2 oxyhalide tellurite glasses for amorphous silicon solar cells, Opt. Mater. 36 (2014) 1040–1043, https://doi.org/10.1016/j.optmat.2014.01.020.

[134] Z.Q. Li, X.D. Li, Q.Q. Liu, X.H. Chen, Z. Sun, C. Liu, X.J. Ye, S.M. Huang, Core/shell structured $NaYF_4$:Yb^{3+}/Er^{3+}/Gd^{+3} nanorods with Au nanoparticles or shells for flexible amorphous silicon solar cells, Nanotechnology 23 (2012), 025402, https://doi.org/10.1088/0957-4484/23/2/025402.

[135] F. Yang, X. Hao, Y. Chen, S. Yang, Luminescence of hydrothermally fabricated PbF_2:Er^{3+} particles and their application in bifacial silicon solar cells, Opt. Appl. XLIV (2014), https://doi.org/10.5277/oa140310.

[136] S. Fischer, B. Fröhlich, H. Steinkemper, K.W. Krämer, J.C. Goldschmidt, Absolute upconversion quantum yield of β-$NaYF_4$ doped with Er^{3+} and external quantum efficiency of upconverter solar cell devices under broad-band excitation considering spectral mismatch corrections, Sol. Energy Mater. Sol. Cells 122 (2014) 197–207, https://doi.org/10.1016/j.solmat.2013.12.001.

[137] S. Chen, G. Zhou, F. Su, H. Zhang, L. Wang, M. Wu, M. Chen, L. Pan, S. Wang, Power conversion efficiency enhancement in silicon solar cell from solution processed transparent upconversion film, Mater. Lett. 77 (2012) 17–20, https://doi.org/10.1016/j.matlet.2012.02.123.

[138] F. Pellé, S. Ivanova, J.-F. Guillemoles, Upconversion of 1.54 μm radiation in Er^{3+} doped fluoride-based materials for c-Si solar cell with improved efficiency, EPJ Photovoltaics 2 (2011) 20601, https://doi.org/10.1051/epjpv/2011002.

[139] S. Fischer, J.C. Goldschmidt, P. Löper, G.H. Bauer, R. Brüggemann, K. Krämer, D. Biner, M. Hermle, S.W. Glunz, Enhancement of Silicon Solar Cell Efficiency by Upconversion: Optical and Electrical Characterization, in: J. Appl. Phys., American Institute of PhysicsAIP, 2010, 044912, https://doi.org/10.1063/1.3478742.

[140] B.S. Richards, A. Shalav, Enhancing the near-infrared spectral response of silicon optoelectronic devices via up-conversion, IEEE Trans. Electron. Dev. 54 (2007) 2679–2684, https://doi.org/10.1109/TED.2007.903197.

[141] J. Dutta, V.K. Rai, Upconverting $BiYO_3$ nanophosphors in DSSCs applications, Opt Laser. Technol. 140 (2021) 107087, https://doi.org/10.1016/j.optlastec.2021.107087.

[142] X. Yang, L. Cai, L. Zhao, Z. Li, C. Wu, J. Sun, Z. Liang, S. Wang, A triple-functional photoanode for light harvesting enhancement in dye sensitized solar cells, Mater. Sci. Semicond. Process. 128 (2021) 105751, https://doi.org/10.1016/j.mssp.2021.105751.

[143] M. Yu, H. Xu, Y. Li, Q. Dai, G. Wang, W. Qin, Morphology luminescence and photovoltaic performance of lanthanide-doped $CaWO_4$ nanocrystals, J. Colloid Interface Sci. 559 (2020) 162–168, https://doi.org/10.1016/j.jcis.2019.10.011.

[144] M. Ambapuram, R. Ramireddy, G. Maddala, S. Godugunuru, P.V.S. Yerva, R. Mitty, Effective upconverter and light scattering dual function $LiYF_4$:Er^{3+}/Yb^{3+} assisted photoelectrode for high performance cosensitized dye sensitized solar cells, ACS Appl. Electron. Mater. 2 (2020) 962–970, https://doi.org/10.1021/acsaelm.0c00014.

[145] P. Tadge, R.S. Yadav, P.K. Vishwakarma, S.B. Rai, T.M. Chen, S. Sapra, S. Ray, Enhanced photovoltaic performance of Y_2O_3:Ho^{3+}/Yb^{3+} upconversion nanophosphor based DSSC and investigation of color tunability in Ho^{3+}/Tm^{3+}/Yb^{3+} tridoped Y_2O_3, J. Alloys Compd. 821 (2020) 153230, https://doi.org/10.1016/j.jallcom.2019.153230.

[146] J. Yu, Y. Yang, C. Zhang, R. Fan, T. Su, Preparation of YbF_3-Ho@TiO_2core-shell sub-microcrystal spheres and their application to the electrode of dye-sensitized solar cells, New J. Chem. 44 (2020) 10545–10553, https://doi.org/10.1039/d0nj02069a.

[147] Z. Hu, L. Zhao, H. Guo, S. Wang, W. Li, X. Yang, B. Dong, L. Wan, Novel double-layered photoanodes based on porous-hollow TiO_2 microspheres and $La(OH)_3$:Yb^{3+}/Er^{3+} for highly efficient dye-sensitized solar cells, J. Mater. Sci. Mater. Electron. 30 (2019) 212–220, https://doi.org/10.1007/s10854-018-0283-7.

[148] M. Qamar, B. Zhang, Y. Feng, Enhanced photon harvesting in dye-sensitized solar cells by doping TiO_2 photoanode with $NaYF_4$:Yb^{3+},Tm^{3+} microrods, Opt. Mater. 89 (2019) 368–374, https://doi.org/10.1016/j.optmat.2019.01.049.

[149] X. Mao, J. Yu, J. Xu, L. Wan, Y. Yang, H. Lin, J. Xu, R. Zhou, Commercial upconversion phosphors with high light harvesting: a superior candidate for high-performance dye-sensitized solar cells, Phys. Status Solidi Appl. Mater. Sci. 216 (2019) 1900382, https://doi.org/10.1002/pssa.201900382.

[150] J. Wang, Z. Du, M. Hojamberdiev, S. Zheng, Y. Xu, Oxalate-assisted morphological effect of $NaYF_4$:Yb^{3+},Er^{3+} on photoelectrochemical performance for dye-sensitized solar cells, J. Rare Earths 36 (2018) 353–358, https://doi.org/10.1016/j.jre.2017.09.008.

[151] T. Chen, Y. Shang, S. Hao, L. Tian, Y. Hou, C. Yang, Enhancement of dye sensitized solar cell efficiency through introducing concurrent upconversion/downconversion core/shell nanoparticles as spectral converters, Electrochim. Acta 282 (2018) 743–749, https://doi.org/10.1016/j.electacta.2018.06.111.

[152] L. Tian, Y. Shang, S. Hao, Q. Han, T. Chen, W. Lv, C. Yang, Constructing a "native" oxyfluoride layer on fluoride particles for enhanced upconversion luminescence, Adv. Funct. Mater. 28 (2018) 1803946, https://doi.org/10.1002/adfm.201803946.

[153] J. Li, O. Yin, L. Zhao, Z. Wang, B. Dong, L. Wan, S. Wang, Enhancing the photoelectric conversion efficiency of dye-sensitized solar cell using the upconversion luminescence materials Y_2O_3:Er^{3+} nanorods doped TiO_2 photoanode, Mater. Lett. 227 (2018) 209–212, https://doi.org/10.1016/j.matlet.2018.05.057.

[154] G. Han, M. Wang, D. Li, J. Bai, G. Diao, Novel upconversion Er, Yb-CeO_2 hollow spheres as scattering layer materials for efficient dye-sensitized solar cells, Sol. Energy Mater. Sol. Cells 160 (2017) 54–59, https://doi.org/10.1016/j.solmat.2016.10.021.

[155] F. Meng, Y. Luo, Y. Zhou, J. Zhang, Y. Zheng, G. Cao, X. Tao, Integrated plasmonic and upconversion starlike Y_2O_3:Er/Au@TiO_2 composite for enhanced photon harvesting in dye-sensitized solar cells, J. Power Sources 316 (2016) 207–214, https://doi.org/10.1016/j.jpowsour.2016.03.032.

[156] N. Chander, A.F. Khan, V.K. Komarala, S. Chawla, V. Dutta, Enhancement of dye sensitized solar cell efficiency via incorporation of upconverting phosphor nanoparticles as spectral converters, Prog. Photovoltaics Res. Appl. 24 (2016) 692–703, https://doi.org/10.1002/pip.2723.

[157] M. Luoshan, L. Bai, C. Bu, X. Liu, Y. Zhu, K. Guo, R. Jiang, M. Li, X. Zhao, Surface plasmon resonance enhanced multi-shell-modified upconversion $NaYF_4$:Yb^{3+}, Er^{3+}@SiO_2@Au@TiO_2 crystallites for dye-sensitized solar cells, J. Power Sources 307 (2016) 468–473, https://doi.org/10.1016/j.jpowsour.2016.01.028.

[158] J. Yu, Y. Yang, R. Fan, P. Wang, Y. Dong, Enhanced photovoltaic performance of dye-sensitized solar cells using a new photoelectrode material: upconversion YbF_3-Ho/TiO_2 nanoheterostructures, Nanoscale 8 (2016) 4173–4180, https://doi.org/10.1039/c5nr08319b.

[159] P. Du, J.H. Lim, S.H. Kim, J.S. Yu, Facile synthesis of Gd_2O_3:Ho^{3+}/Yb^{3+} nanoparticles: an efficient upconverting material for enhanced photovoltaic performance of dye-sensitized solar cells, Opt. Mater. Express 6 (2016) 1896, https://doi.org/10.1364/ome.6.001896.

[160] P. Padhye, S. Sadhu, M. Malik, P. Poddar, A broad spectrum photon responsive, paramagnetic: β -$NaGdF_4$:Yb^{3+},Er^{3+}-mesoporous anatase titania nanocomposite, RSC Adv. 6 (2016) 53504–53518, https://doi.org/10.1039/c6ra06813h.

[161] X. Jin, H. Li, D. Li, Q. Zhang, F. Li, W. Sun, Z. Chen, Q. Li, Role of ytterbium-erbium co-doped gadolinium molybdate ($Gd_2(MoO_4)_3$:Yb/Er) nanophosphors in solar cells, Opt Express 24 (2016) A1276, https://doi.org/10.1364/oe.24.0a1276.

[162] Y. Wang, Y. Zhu, X. Yang, J. Shen, X. Li, S. Qian, C. Li, Performance optimization in dye-sensitized solar cells with β-$NaYF_4$:Yb^{3+},Er^{3+}@SiO_2@TiO_2 mesoporous microspheres as multi-functional photoanodes, Electrochim. Acta 211 (2016) 92–100, https://doi.org/10.1016/j.electacta.2016.05.216.

[163] M. Luoshan, M. Li, X. Liu, K. Guo, L. Bai, Y. Zhu, B. Sun, X. Zhao, Performance optimization in dye-sensitized solar cells with β-$NaYF_4$:Er^{3+}/Yb^{3+} and graphene multi-functional layer hybrid composite photoanodes, J. Power Sources 287 (2015) 231–236, https://doi.org/10.1016/j.jpowsour.2015.04.068.

[164] Y.M. Kim, C.S. Kim, H.W. Choi, Efficiency improvement of dye-sensitized solar cells by phosphor (Y_2O_3:Er^{3+}, $Y_3Al_5O_{12}$:Ce^{3+}) co-doped TiO_2 electrodes, Mol. Cryst. Liq. Cryst. 620 (2015) 83–90, https://doi.org/10.1080/15421406.2015.1094874.

[165] Y. Liu, Y. Xia, Y. Jiang, M. Zhang, W. Sun, X.Z. Zhao, Coupling effects of Au-decorated core-shell β-$NaYF_4$:Er/Yb@SiO_2 microprisms in dye-sensitized solar cells: plasmon resonance versus upconversion, Electrochim. Acta 180 (2015) 394–400, https://doi.org/10.1016/j.electacta.2015.08.144.

[166] J. Bai, R. Zhao, G. Han, Z. Li, G. Diao, Synthesis of 1D upconversion CeO_2:Er,Yb nanofibers via electrospinning and their performance in dye-sensitized solar cells, RSC Adv. 5 (2015) 43328–43333, https://doi.org/10.1039/c5ra06917c.

[167] W. Liao, D. Zheng, J. Tian, Z. Lin, Dual-functional semiconductor-decorated upconversion hollow spheres for high efficiency dye-sensitized solar cells, J. Mater. Chem. 3 (2015) 23360–23367, https://doi.org/10.1039/c5ta06238a.

[168] K. Wang, J. Jiang, S. Wan, J. Zhai, Upconversion enhancement of lanthanide-doped $NaYF_4$ for quantum dot-sensitized solar cells, Electrochim. Acta 155 (2015) 357–363, https://doi.org/10.1016/j.electacta.2014.11.131.

[169] P. Du, J.H. Lim, J.W. Leem, S.M. Cha, J.S. Yu, Enhanced photovoltaic performance of dye-sensitized solar cells by efficient near-infrared sunlight harvesting using upconverting Y_2O_3:Er^{3+}/Yb^{3+} phosphor nanoparticles, Nanoscale Res. Lett. 10 (2015) 321, https://doi.org/10.1186/s11671-015-1030-0.

[170] N. Yao, J. Huang, K. Fu, X. Deng, M. Ding, M. Shao, X. Xu, Enhanced light harvesting of dye-sensitized solar cells with up/down conversion materials, Electrochim. Acta 154 (2015) 273–277, https://doi.org/10.1016/j.electacta.2014.12.095.

[171] N.C. Dyck, G.P. Demopoulos, Integration of upconverting β-$NaYF_4$:Yb^{3+},Er^{3+}@TiO_2 composites as light harvesting layers in dye-sensitized solar cells, RSC Adv. 4 (2014) 52694–52701, https://doi.org/10.1039/c4ra08775e.

[172] C. Yuan, G. Chen, L. Li, J.A. Damasco, Z. Ning, H. Xing, T. Zhang, L. Sun, H. Zeng, A.N. Cartwright, P.N. Prasad, H. Ågren, Simultaneous multiple wavelength upconversion in a core-shell nanoparticle for enhanced near infrared light harvesting in a dye-sensitized solar cell, ACS Appl. Mater. Interfaces 6 (2014) 18018–18025, https://doi.org/10.1021/am504866g.

[173] Z. Zhou, J. Wang, F. Nan, C. Bu, Z. Yu, W. Liu, S. Guo, H. Hu, X.Z. Zhao, Upconversion induced enhancement of dye sensitized solar cells based on core-shell structured β-$NaYF_4$:Er^{3+},Yb^{3+}@SiO_2 nanoparticles, Nanoscale 6 (2014) 2052–2055, https://doi.org/10.1039/c3nr04315k.

[174] J. Yu, Y. Yang, R. Fan, D. Liu, L. Wei, S. Chen, L. Li, B. Yang, W. Cao, Enhanced near-infrared to visible upconversion nanoparticles of Ho^{3+}-Yb^{3+}-F- tri-doped TiO_2 and its application in dye-sensitized solar cells with 37% improvement in power conversion efficiency, Inorg. Chem. 53 (2014) 8045–8053, https://doi.org/10.1021/ic501041h.

[175] L. Li, Y. Yang, R. Fan, Y. Jiang, L. Wei, Y. Shi, J. Yu, S. Chen, P. Wang, B. Yang, W. Cao, A simple modification of near-infrared photon-to-electron response with fluorescence resonance energy transfer for dye-sensitized solar cells, J. Power Sources 264 (2014) 254–261, https://doi.org/10.1016/j.jpowsour.2014.04.100.

[176] P. Zhao, Y. Zhu, X. Yang, X. Jiang, J. Shen, C. Li, Plasmon-enhanced efficient dye-sensitized solar cells using core–shell-structured β-$NaYF_4$:Yb,Er@SiO_2@Au nanocomposites, J. Mater. Chem. 2 (2014) 16523–16530, https://doi.org/10.1039/C4TA02230K.

[177] L. Liang, Y. Liu, C. Bu, K. Guo, W. Sun, N. Huang, T. Peng, B. Sebo, M. Pan, W. Liu, S. Guo, X.Z. Zhao, Highly uniform, bifunctional core/double-shell-structured β-$NaYF_4$:Er^{3+},Yb^{3+}@SiO_2@TiO_2 hexagonal sub-microprisms for high-

performance dye sensitized solar cells, Adv. Mater. 25 (2013) 2174–2180, https://doi.org/10.1002/adma.201204847.
[178] L. Liang, Y. Yulin, Z. Mi, F. Ruiqing, Q. Lele, W. Xin, Z. Lingyun, Z. Xuesong, H. Jianglong, Enhanced performance of dye-sensitized solar cells based on TiO_2 with NIR-absorption and visible upconversion luminescence, J. Solid State Chem. 198 (2013) 459–465, https://doi.org/10.1016/j.jssc.2012.10.013.
[179] J. Yu, Y. Yang, R. Fan, H. Zhang, L. Li, L. Wei, Y. Shi, K. Pan, H. Fu, Er^{3+} and Yb^{3+} co-doped $TiO_{2-x}F_x$ up-conversion luminescence powder as a light scattering layer with enhanced performance in dye sensitized solar cells, J. Power Sources 243 (2013) 436–443, https://doi.org/10.1016/j.jpowsour.2013.06.014.
[180] J. Zhang, H. Shen, W. Guo, S. Wang, C. Zhu, F. Xue, J. Hou, H. Su, Z. Yuan, An upconversion $NaYF_4$:Yb^{3+},Er^{3+}/TiO_2 core-shell nanoparticle photoelectrode for improved efficiencies of dye-sensitized solar cells, J. Power Sources 226 (2013) 47–53, https://doi.org/10.1016/j.jpowsour.2012.10.073.
[181] Y. Li, G. Wang, K. Pan, B. Jiang, C. Tian, W. Zhou, H. Fu, $NaYF_4$:Er^{3+}/Yb^{3+}-graphene composites: preparation, upconversion luminescence, and application in dye-sensitized solar cells, J. Mater. Chem. 22 (2012) 20381–20386, https://doi.org/10.1039/c2jm34113a.
[182] J. Wang, J. Wu, J. Lin, M. Huang, Y. Huang, Z. Lan, Y. Xiao, G. Yue, S. Yin, T. Sato, Application of Y_2O_3:Er^{3+} nanorods in dye-sensitized solar cells, ChemSusChem 5 (2012) 1307–1312, https://doi.org/10.1002/cssc.201100596.
[183] A.F. Khan, R. Yadav, P.K. Mukhopadhya, S. Singh, C. Dwivedi, V. Dutta, S. Chawla, Core-shell nanophosphor with enhanced NIR-visible upconversion as spectrum modifier for enhancement of solar cell efficiency, J. Nanoparticle Res. 13 (2011) 6837–6846, https://doi.org/10.1007/s11051-011-0591-9.
[184] G.X. Xie, J.M. Lin, J.H. Wu, Z. Lan, Q.H. Li, Y.M. Xiao, G.T. Yue, H.F. Yue, M. L. Huang, Application of upconversion luminescence in dye-sensitized solar cells, Chin. Sci. Bull. 56 (2011) 96–101, https://doi.org/10.1007/s11434-010-4115-2.
[185] Q. Li, J. Lin, J. Wu, Z. Lan, Y. Wang, F. Peng, M. Huang, Enhancing photovoltaic performance of dye-sensitized solar cell by rare-earth doped oxide of Lu_2O_3:(Tm^{3+}, Yb^{3+}), Electrochim. Acta 56 (2011) 4980–4984, https://doi.org/10.1016/j.electacta.2011.03.125.
[186] G. Bin Shan, H. Assaaoudi, G.P. Demopoulos, Enhanced performance of dye-sensitized solar cells by utilization of an external, bifunctional layer consisting of uniform β-$NaYF_4$:Er^{3+}/Yb^{3+} nanoplatelets, ACS Appl. Mater. Interfaces 3 (2011) 3239–3243, https://doi.org/10.1021/am200537e.
[187] J. Wu, J. Wang, J. Lin, Z. Lan, Q. Tang, M. Huang, Y. Huang, L. Fan, Q. Li, Z. Tang, Enhancement of the photovoltaic performance of dye-sensitized solar cells by doping $Y_{0.78}Yb_{0.20}Er_{0.02}F_3$ in the photoanode, Adv. Energy Mater. 2 (2012) 78–81, https://doi.org/10.1002/aenm.201100531.
[188] F. Xu, Y. Sun, H. Gao, S. Jin, Z. Zhang, H. Zhang, G. Pan, M. Kang, X. Ma, Y. Mao, High-performance perovskite solar cells based on $NaCsWO_3$@$NaYF_4$@$NaYF_4$:Yb, Er upconversion nanoparticles, ACS Appl. Mater. Interfaces 13 (2021) 2674–2684, https://doi.org/10.1021/acsami.0c19475.
[189] W. Bi, Y. Wu, C. Chen, D. Zhou, Z. Song, D. Li, G. Chen, Q. Dai, Y. Zhu, H. Song, Dye sensitization and local surface plasmon resonance-enhanced upconversion luminescence for efficient perovskite solar cells, ACS Appl. Mater. Interfaces 12 (2020) 24737–24746, https://doi.org/10.1021/acsami.0c04258.
[190] L. Wang, K. Chen, H. Tong, K. Wang, L. Tao, Y. Zhang, X. Zhou, Inverted pyramid Er^{3+} and Yb^{3+} Co-doped TiO_2 nanorod arrays based perovskite solar cell: infrared response and improved current density, Ceram. Int. 46 (2020) 12073–12079, https://doi.org/10.1016/j.ceramint.2020.01.249.
[191] Q. Guo, J. Wu, Y. Yang, X. Liu, J. Jia, J. Dong, Z. Lan, J. Lin, M. Huang, Y. Wei, Y. Huang, High performance perovskite solar cells based on β-$NaYF_4$:Yb^{3+}/Er^{3+}/Sc^{3+}@$NaYF_4$ core-shell upconversion nanoparticles, J. Power Sources 426 (2019) 178–187, https://doi.org/10.1016/j.jpowsour.2019.04.039.
[192] H. Zhang, Y. Xiao, F. Qi, P. Liu, Y. Wang, F. Li, C. Wang, G. Fang, X. Zhao, Near-infrared light-sensitive hole-transport-layer free perovskite solar cells and photodetectors with hexagonal $NaYF_4$:Yb^{3+},Tm^{3+}@SiO_2 upconversion nanoprism-modified TiO_2 scaffold, ACS Sustain. Chem. Eng. 7 (2019) 8236–8244, https://doi.org/10.1021/acssuschemeng.8b06606.
[193] D. Ma, Y. Shen, T. Su, J. Zhao, N.U. Rahman, Z. Xie, F. Shi, S. Zheng, Y. Zhang, Z. Chi, Performance enhancement in up-conversion nanoparticle-embedded perovskite solar cells by harvesting near-infrared sunlight, Mater. Chem. Front. 3 (2019) 2058–2065, https://doi.org/10.1039/c9qm00311h.
[194] H. Zhang, Q. Zhang, Y. Lv, C. Yang, H. Chen, X. Zhou, Upconversion Er-doped TiO_2 nanorod arrays for perovskite solar cells and the performance improvement, Mater. Res. Bull. 106 (2018) 346–352, https://doi.org/10.1016/j.materresbull.2018.06.014.
[195] Y. Li, L. Zhao, M. Xiao, Y. Huang, B. Dong, Z. Xu, L. Wan, W. Li, S. Wang, Synergic effects of upconversion nanoparticles $NaYbF_4$:Ho^{3+} and ZrO_2 enhanced the efficiency in hole-conductor-free perovskite solar cells, Nanoscale 10 (2018) 22003–22011, https://doi.org/10.1039/c8nr07225f.
[196] Z. Zhang, J. Qin, W. Shi, Y. Liu, Y. Zhang, Y. Liu, H. Gao, Y. Mao, Enhanced power conversion efficiency of perovskite solar cells with an up-conversion material of Er^{3+}-Yb^{3+}-Li^+ tri-doped TiO_2, Nanoscale Res. Lett. 13 (2018) 147, https://doi.org/10.1186/s11671-018-2545-y.
[197] J. Hu, Y. Qiao, Y. Yang, L. Zhao, W. Liu, S. Li, P. Liu, M. Chen, Enhanced performance of hole-conductor-free perovskite solar cells by utilization of core/shell-structured β-$NaYF_4$:Yb^{3+},Er^{3+}@SiO_2 nanoparticles in ambient air, IEEE J. Photovoltaics 8 (2018) 132–136, https://doi.org/10.1109/JPHOTOV.2017.2762585.
[198] X. Wang, Z. Zhang, J. Qin, W. Shi, Y. Liu, H. Gao, Y. Mao, Enhanced photovoltaic performance of perovskite solar cells based on Er-Yb Co-doped TiO_2 nanorod arrays, Electrochim. Acta 245 (2017) 839–845, https://doi.org/10.1016/j.electacta.2017.06.032.
[199] Y. Ding, H. Qiao, T. Yang, N. Yin, P. Li, Y. Zhao, X. Zhang, Upconversion luminescence co-enhanced by Li^+ ions doping and localized surface plasmon resonance for perovskite solar cells, Opt. Mater. 73 (2017) 617–622, https://doi.org/10.1016/j.optmat.2017.09.012.
[200] X. Lai, X. Li, X. Lv, Y.Z. Zheng, F. Meng, X. Tao, Broadband dye-sensitized upconverting nanocrystals enabled near-infrared planar perovskite solar cells, J. Power Sources 372 (2017) 125–133, https://doi.org/10.1016/j.jpowsour.2017.10.067.
[201] D. Zhou, D. Liu, J. Jin, X. Chen, W. Xu, Z. Yin, G. Pan, D. Li, H. Song, Semiconductor plasmon-sensitized broadband upconversion and its enhancement effect on the power conversion efficiency of perovskite solar cells, J. Mater. Chem. 5 (2017) 16559–16567, https://doi.org/10.1039/c7ta04943a.
[202] J. Roh, H. Yu, J. Jang, Hexagonal β-$NaYF_4$:Yb^{3+},Er^{3+} nanoprism-incorporated upconverting layer in perovskite solar cells for near-infrared sunlight harvesting, ACS Appl. Mater. Interfaces 8 (2016), https://doi.org/10.1021/acsami.6b04760, 19847–19852.
[203] M. Que, W. Que, X. Yin, P. Chen, Y. Yang, J. Hu, B. Yu, Y. Du, Enhanced conversion efficiency in perovskite solar cells by effectively utilizing near infrared light, Nanoscale 8 (2016) 14432–14437, https://doi.org/10.1039/c6nr03021a.
[204] J.P. Guerrero-Jimenez, V.H.R. Arellano, I. Zarazua, T. Lopez-Luke, R. Doddoji, A. Cerdan-Pasaran, Increase the quantum dots sensitized TiO_2 solar cell efficiency adding n%Yb^{3+} −1%Er^{3+} doped $NaYF_4$: submicrometer-sized rods, IEEE J. Photovoltaics 10 (2020) 785–794, https://doi.org/10.1109/JPHOTOV.2020.2971141.
[205] P. Qu, K. Wang, J. Li, S. Wang, W. Wei, Upconverting TiO_2 spheres with light scattering effect for enhanced quantum dot-sensitized solar cells, Mater. Express. 10 (2020) 556–562, https://doi.org/10.1166/mex.2020.1672.
[206] H. Chen, S.M. Lee, A. Montenegro, D. Kang, B. Gai, H. Lim, C. Dutta, W. He, M. L. Lee, A. Benderskii, J. Yoon, Plasmonically enhanced spectral upconversion for improved performance of GaAs solar cells under nonconcentrated solar illumination, ACS Photonics 5 (2018) 4289–4295, https://doi.org/10.1021/acsphotonics.8b01245.
[207] S. Chen, B. Peng, F. Lu, Y. Mei, F. Cheng, L. Deng, Q. Xiong, L. Wang, X. Sun, W. Huang, Scattering or photoluminescence? Major mechanism exploration on performance enhancement in P3HT-based polymer solar cells with $NaYF_4$:2%Er^{3+},18%Yb^{3+} upconverting nanocrystals, Adv. Opt. Mater. 2 (2014) 442–449, https://doi.org/10.1002/adom.201300522.
[208] J.L. Wu, F.C. Chen, S.H. Chang, K.S. Tan, H.Y. Tuan, Upconversion effects on the performance of near-infrared laser-driven polymer photovoltaic devices, Org. Electron. 13 (2012) 2104–2108, https://doi.org/10.1016/j.orgel.2012.05.057.
[209] A.A.D. Adikaari, I. Etchart, P.H. Guéring, M. Bérard, S.R.P. Silva, A.K. Cheetham, R.J. Curry, Near infrared up-conversion in organic photovoltaic devices using an efficient Yb^{3+}:Ho^{3+} co-doped Ln_2BaZnO_5 (Ln Y, Gd) phosphor, J. Appl. Phys. 111 (2012), 094502, https://doi.org/10.1063/1.4704687.
[210] H.-Y. Lin, H.-N. Chen, T.-H. Wu, C.-S. Wu, Y.-K. Su, S.-Y. Chu, Investigation of green up-conversion behavior in $Y_6W_2O_{15}$:Yb^{3+},Er^{3+} phosphor and its verification in 973-nm laser-driven GaAs solar cell, J. Am. Ceram. Soc. 95 (2012) 3172–3179, https://doi.org/10.1111/j.1551-2916.2012.05281.x.
[211] A. Richter, R. Müller, J. Benick, F. Feldmann, B. Steinhauser, C. Reichel, A. Fell, M. Bivour, M. Hermle, S.W. Glunz, Design rules for high-efficiency both-sides-contacted silicon solar cells with balanced charge carrier transport and recombination losses, Nat. Energy 6 (2021) 429–438, https://doi.org/10.1038/s41560-021-00805-w.
[212] M. Köhler, M. Pomaska, P. Procel, R. Santbergen, A. Zamchiy, B. Macco, A. Lambertz, W. Duan, P. Cao, B. Klingebiel, S. Li, A. Eberst, M. Luysberg, K. Qiu, O. Isabella, F. Finger, T. Kirchartz, U. Rau, K. Ding, A silicon carbide based highly transparent passivating contact for crystalline silicon solar cells approaching efficiencies of 24%, Nat. Energy 6 (2021) 529–537, https://doi.org/10.1038/s41560-021-00806-9.
[213] J.A. Van Delft, D. Garcia-Alonso, W.M.M. Kessels, Atomic layer deposition for photovoltaics: Applications and prospects for solar cell manufacturing, Semicond. Sci. Technol. 27 (2012), 074002, https://doi.org/10.1088/0268-1242/27/7/074002.
[214] V. Zardetto, B.L. Williams, A. Perrotta, F. Di Giacomo, M.A. Verheijen, R. Andriessen, W.M.M. Kessels, M. Creatore, Atomic layer deposition for perovskite solar cells: research status, opportunities and challenges, Sustain. Energy Fuels 1 (2017) 30–55, https://doi.org/10.1039/c6se00076b.
[215] M. Leskelä, K. Kukli, M. Ritala, Rare-earth oxide thin films for gate dielectrics in microelectronics, J. Alloys Compd. 418 (2006) 27–34, https://doi.org/10.1016/j.jallcom.2005.10.061.